Title
Performance Bounds on Spatial Coverage Tasks by Stochastic Robotic Swarms

Journal
IEEE Transactions on Automatic Control, 63(6)

ISSN
0018-9286

Authors
Zhang, Fangbo
Bertozzi, Andrea L
Elamvazhuthi, Karthik
et al.

Publication Date
2018

DOI
10.1109/tac.2017.2747769

Peer reviewed

Performance Bounds on Spatial Coverage Tasks by Stochastic Robotic Swarms

Fangbo Zhang, Andrea L. Bertozzi, Karthik Elamvazhuthi, and Spring Berman, *Member, IEEE*

***Abstract*—This paper presents a novel procedure for computing parameters of a robotic swarm that guarantee coverage performance by the swarm within a specified error from a target spatial distribution. The main contribution of this paper is the analysis of the dependence of this error on two key parameters: the number of robots in the swarm and the robot sensing radius. The robots cannot localize or communicate with one another, and they exhibit stochasticity in their motion and task-switching policies. We model the population dynamics of the swarm as an advection-diffusion-reaction partial differential equation (PDE) with time-dependent advection and reaction terms. We derive rigorous bounds on the discrepancies between the target distribution and the coverage achieved by individual-based and PDE models of the swarm. We use these bounds to select the swarm size that will achieve coverage performance within a given error and the corresponding robot sensing radius that will minimize this error. We also apply the optimal control approach from our prior work in [13] to compute the robots' velocity field and task-switching rates. We validate our procedure through simulations of a scenario, in which a robotic swarm must achieve a specified density of pollination activity over a crop field.**

***Index Terms*—Advection-diffusion-reaction (ADR) partial differential equation (PDE), optimal control, stochastic systems, swarm robotics.**

I. Introduction

IN RECENT years, there has been a growing interest in the development of *robotic swarms* [7] for a range of applications, including environmental sensing, exploration, mapping, disaster response, surveillance, cooperative manipulation, and even nanomedicine [29]. Indeed, advances in manufacturing, computing, sensing, actuation, control, and other technologies have already enabled the development of a variety of low-cost robotic platforms that can be deployed in large numbers, e.g., [9], [16], [20].

Manuscript received June 1, 2017; revised August 6, 2017; accepted August 15, 2017. Date of publication August 31, 2017; date of current version May 23, 2018. This work was supported in part by the National Science Foundation under Award CMMI-1435709 and Award CMMI-1436960. Recommended by Associate Editor E. Cerpa. *(Corresponding author: Fangbo Zhang.)*

F. Zhang and A. L. Bertozzi are with the Department of Mathematics, University of California, Los Angeles, CA 90095 USA (e-mail: fbzhang2013@math.ucla.edu; bertozzi@math.ucla.edu).

K. Elamvazhuthi and S. Berman are with the School for Engineering of Matter, Transport and Energy, Arizona State University, Tempe, AZ 85287 USA (e-mail: karthikevaz@asu.edu; spring.berman@asu.edu).

Color versions of one or more of the figures in this paper are available online at http://ieeexplore.ieee.org.

Digital Object Identifier 10.1109/TAC.2017.2747769

While the technology to create robotic swarms is progressing, it remains a challenge to predict and control these systems' collective behaviors when they operate in uncertain, unstructured, GPS-denied environments. Another constraint is that interrobot communication may need to be minimized or excluded in order to conserve power and reduce the possibility of detection by adversaries. Importantly, control policies and verification methods for robotic swarms must accommodate *nondeterministic behaviors* that arise in autonomous systems [1]. Stochasticity in robots' motion and decisions can arise from inherent sensor and actuator noise, especially in small highly resource-restricted platforms. Stochasticity may also be intentionally introduced, for example, when robots are programed to perform random walks for probabilistic search and tracking missions [28], or to switch probabilistically between behavioral states or tasks in a manner similar to social insects. Social insect colonies provide a useful paradigm for robotic swarm control in that they display robust collective behaviors that emerge from the decentralized decisions of numerous individuals, which act on locally perceived information [6].

Control methodologies for robotic swarms should be scalable with the number of robots and reliant on limited human supervision, since situational awareness decreases with large robot populations. Toward this end, we employ a methodology that is based on models of the robots' decision making and motion at multiple levels of abstraction. The multilevel modeling framework is adopted from the disciplines of stochastic chemical kinetics and fluid dynamics, and it has been used by the authors and others, e.g., in [13], [17], [27], to describe the population dynamics of large numbers of robots. This framework has also been used to model collective behaviors in biological swarms, such as flocking, schooling, chemotaxis, pattern formation, and predator–prey interactions [24].

In our modeling framework, the *microscopic model* is a discrete model that represents the actions of individual robots. We consider swarms of robots that display stochastic motion and decision making as described above, while also moving according to a programed deterministic velocity field. Each robot's stochastic movement can be modeled as a Brownian motion with an associated diffusion coefficient. Since the motion of each robot consists of a deterministic advection and a stochastic Brownian walk, it is governed by a stochastic differential equation (SDE). A robot's stochastic transition between two behavioral states can be modeled as a chemical reaction with a programmable transition probability rate.

Implementations of the microscopic model can be computationally expensive to simulate, requiring exhaustive parametric studies, and intractable for analysis as the number of robots increases. To overcome these limitations, the microscopic model can be abstracted to a lower dimensional continuum

representation, the *macroscopic model*, which consists of a set of advection-diffusion-reaction (ADR) partial differential equations (PDEs). These equations govern the spatiotemporal dynamics of *density fields* of robots in different behavioral states. The macroscopic model enables a quantitative characterization of population behaviors, since it is amenable to analytical treatment and numerical experiments. In addition, techniques for control and optimization of PDEs can be applied to compute values of the model parameters that produce a desired global objective. These parameters define the robots' programmable control policies for motion and state transitions, and the resulting collective behavior of the robots follows the macroscopic model prediction in expectation. Scalability of this "top-down" control approach is ensured by the fact that the dimensionality of the macroscopic model is independent of the number of robots. Human supervisory control can be exercised in the specification of the global objective and the set of tunable model parameters and state transitions.

In recent years, there have been various applications of control-theoretic techniques to PDE macroscopic models of multiagent systems for the purpose of synthesizing agent controllers that produce desired collective behaviors. ADR PDE models, in particular, have been used by the authors to design robot control policies that achieve target spatial distributions of robot activity over a bounded domain [13] and that drive the swarm to a distribution that is proportional to a locally measured scalar field [12]. ADR PDEs have also been used to control the probability density functions (pdfs) of multidimensional stochastic processes [2], develop multiagent coverage and search strategies that are inspired by bacterial chemotaxis [22], and maximize the probability of swarm robotic presence in a desired region [23]. Other work on PDE-based analysis and design of agent control laws includes a study of multiagent consensus protocols in an Eulerian framework [8]; strategies for confining a population of agents, represented as a continuum, with a few discrete leader agents [10]; and an approach to flocking control for a group of agents governed by the kinetic Cucker–Smale model [26].

The literature above addresses the problem of designing the rules that govern robots' behaviors and decisions. However, there has been relatively little effort toward a principled approach to determining the *required number of robots* and *optimal robot specifications*, such as sensing and communication ranges, for a desired collective task. An impediment to developing such an approach is the absence of a rigorous, generalizable analysis of the correspondence between continuum and discrete models of a swarm [3]. Recent work on mean field games [5], [15], [19] demonstrates the convergence of optimal controls of a large number of agents to optimal controls of a mean-field limit system. However, the work does not analyze the convergence of the agent-based model to the mean-field model for a fixed set of controls.

In this paper, we address this challenge for robotic swarms that can be modeled as ADR PDEs at the macroscopic level. We derive a rigorous error bound on the discrepancy between the microscopic and macroscopic models, which depends on the swarm population size (alternatively, the number of swarm deployments), the robot sensing radius length, and the time discretization of the microscopic and macroscopic models. Our derivation employs a representation of each robot as a circular "blob function" [11], [21] with a small parameter that represents the robot's maximum sensing radius. We formulate the discrete density functions of robots in different states and robots' cumulative activity over the domain by summing all of the corresponding blobs. We show that as the number of robots approaches infinity, the discrete density functions converge to the continuous solution of the macroscopic model. We illustrate our approach for a simulated scenario in which a swarm of microaerial vehicles must pollinate a crop field, similar to the problem in [13]. We apply the optimal control approach in [13] to compute vehicle control policies that achieve a target spatial distribution of pollination. We also use our derived error bound to estimate the required swarm size that will achieve the target pollination distribution within a specified percentage of accuracy. In addition, we demonstrate the effect of the maximum sensing radius on the swarm performance and show that an optimal radius length exists for a given swarm size. Notably, the analysis performed here can also be applied to other stochastic control strategies for robotic swarms, such as [12], [17], and [27].

In summary, the contribution of this paper is twofold.

1) We provide a rigorous analysis of the error bound between the aforementioned microscopic and macroscopic models, which is still absent in the literature on stochastic control of multiagent systems with state transitions. This analysis, together with our optimal control approach in [13] which approximates the target distribution using the macroscopic model, provides a formal mathematical validation of our swarm control strategy.
2) Based on the scaling laws that are observed in the error estimates, we propose a principled approach to determine the *required number of robots* and *optimal robot sensing radius* that will achieve a target distribution within a specified error.

This paper is organized as follows. Section II describes our task objective and the robot capabilities and behaviors, and Section III outlines our design procedure for computing the number of robots and the robots' sensing radius, velocity, and pollination rates. Section IV defines the microscopic model, the blob function, and the actual density fields of robots and their pollination activity, and Section V formulates the macroscopic model, an operator splitting method for numerically solving this model, and the expected density fields. Section VI summarizes our optimal control approach, first presented in [13], to designing robot control policies for target spatial coverage. In Section VII, we provide our convergence analysis of the estimated error between the actual, expected, and target density fields. We validate our analysis and design procedure with simulations in Section VIII and conclude in Section IX.

II. Task Objective

In this section, we present the task objective of the robot control scenario defined in [13], which is the basis of the analysis in our paper. We consider a crop field $\Omega \in \mathbb{R}^2$ with several rows of flowers to be pollinated by a swarm of N microaerial vehicles. There are n_f types of crops in the field, and $\Gamma_j \subset \Omega$ denotes the region of the field that is occupied by crops of type $j \in \{1, ..., n_f\}$. The *task objective*, which must be completed within time T, is to achieve a spatial distribution of pollination activity over the field within a specified error γ_d relative to a target pollination distribution $\rho_\Omega(\boldsymbol{x})$, where $\boldsymbol{x} \in \Omega$.

The swarm originates from a location in the field called the *hive*. The robots are assumed to have sufficient power to

undertake brief flights from the hive, and they return to the hive to recharge after a complete flight. Each robot is equipped with a compass and thus can fly with a specified heading. However, the robots' stringent power constraints make it infeasible for them to use interrobot communication or GPS sensors for global localization. A computer in the hive serves as a supervisory agent and calculates the parameters of the robots' motion and state transitions prior to their flight.

Each robot $i \in \{1, ..., N\}$ performs the following actions during a flight. Upon deploying from the hive, each robot flies with a combination of a time-dependent velocity field $\boldsymbol{v}(t) \in \mathbb{R}^2$ and a Brownian motion, which is characterized by a diffusion coefficient parameter $D > 0$. We assume that the flowers are distributed densely enough such that a robot can always detect at least one flower within its sensing radius δ when it flies over the crop rows. The sensing radius can be adjusted within a maximum radius, which is determined by the capability of the robot. When a robot is flying over crops of type j, it decides with a time-dependent probability per unit time $k_j(t)$, the *pollination rate*, to pause at a flower within its sensing range and hover for pollination. The robot resumes flying with a fixed probability per unit time k_f, which determines the time taken to pollinate.

III. Design Procedure for Target Performance Bounds

Here, we present a procedure for computing the number of robots N, the robot velocity $\boldsymbol{v}(t)$, and the robot pollination rates $k_j(t)$ and selecting the robot sensing radius δ to achieve the task objective defined in Section II. The details of certain steps in the procedure are given in subsequent sections, as referenced below. We illustrate this computational procedure in Section VIII for an example pollination scenario.

1) Set values of the parameters n_f, Γ_j, T, $\rho_\Omega(\boldsymbol{x})$, γ_d, D, and k_f, defined in Section II, and Δt and $\boldsymbol{X}_0$, defined in Section IV.
2) Compute the robot control parameters $\boldsymbol{v}(t)$ and $k_j(t)$, defined in Section II, by applying the optimal control technique described in Section VI to the macroscopic model, defined in Section V.
3) Choose a value of δ and two values of N. Simulate the microscopic model, defined in Section IV, for each value of N with the chosen δ and the computed control parameters $\boldsymbol{v}(t)$ and $k_j(t)$.
4) For each value of N, compare the actual distribution of pollination in the microscopic model to the target distribution $\rho_\Omega(\boldsymbol{x})$ and compute the discrepancy between them.
5) Use the convergence analysis in Section VII to estimate the required N such that the discrepancy is less than γ_d.
6) Simulate the microscopic model for several values of δ with the estimate of the required N, and select the δ that yields the minimum discrepancy.

IV. Microscopic Model

A. Robot Controller

We use the same robot controller as in our previous work [13]. We discretize the time span of swarm deployment $[0, T]$ into M equal time steps

$$0 = t_0 < t_1 < \cdots < t_M = T, \quad t_m = m\Delta t. \tag{1}$$

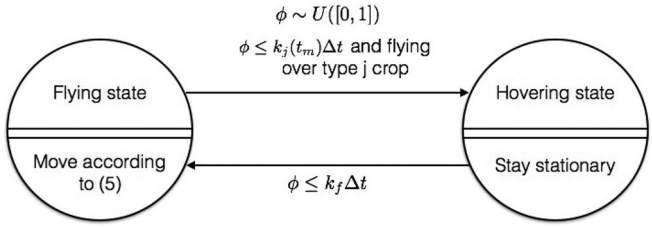

Fig. 1. State-transition diagram of robot controller for pollination. The diagram outlines a program that would run on a single robot.

The controller that drives each robot is illustrated by the state-transition diagram in Fig. 1. Robots switch stochastically between two states: *Flying* and *Hovering*. We define the index sets of robots in each state at time t_m:

$$F_m = \{i : \text{Robot } i \text{ is } Flying\}$$

$$H_{j,m} = \{i : \text{Robot } i \text{ is } Hovering \text{ over crops of type } j\}.$$

All of the robots start from $\boldsymbol{X}_0 \in \Omega$ in the *Flying* state. At the start of each time step Δt, each *Flying* robot that is over crops of type j switches to *Hovering* at a flower with probability $k_j(t_m)\Delta t$, and each *Hovering* robot returns to *Flying* with probability $k_f \Delta t$. We choose Δt to be small enough such that $k_j(t_m)\Delta t \le 1$ and $k_f \Delta t \le 1$, since these probabilities can at most be 1. The robots' state transitions can be modeled as the following reactions, where $\phi \in [0, 1]$ is a uniformly distributed random number:

$$\begin{aligned} i \in F_m &\xrightarrow{\text{if } \phi \le k_j(t_m)\Delta t} i \in H_{j,m+1} \\ i \in H_{j,m} &\xrightarrow{\text{if } \phi \le k_f \Delta t} i \in F_{m+1}. \end{aligned} \tag{2}$$

After generating ϕ and switching states if ϕ satisfies the condition associated with its possible reaction in (2), each robot executes the motion controller that is defined for its current state over the duration Δt. We define the domain as unbounded, and robots may exit and re-enter the bounded subregion of the domain that represents the crop field. The position of robot i at time t_m, the beginning of the time step, is denoted by $\boldsymbol{X}_m^i \in \mathbb{R}^2$. Each *Hovering* robot stays at the location of the flower that it is pollinating, i.e.,

$$\boldsymbol{X}_{m+1}^i = \boldsymbol{X}_m^i \, \forall i \in \cup_{j=1}^{n_f} H_{j,m+1}. \tag{3}$$

Each *Flying* robot moves according to the SDE

$$d\boldsymbol{X}(t) = \boldsymbol{v}(t)\Delta t + \sqrt{2D}\, d\boldsymbol{B}(t) \tag{4}$$

where $\boldsymbol{B}(t)$ is the standard Brownian motion. We simulate this motion using a first-order discretization of (4)

$$\boldsymbol{X}_{m+1}^i = \boldsymbol{X}_m^i + \boldsymbol{v}(t_m)\Delta t + \sqrt{2D\Delta t}\,\Delta \boldsymbol{Z}_m^i \, \forall i \in F_{m+1} \tag{5}$$

where $\Delta \boldsymbol{Z}_m^i$ are independent normally distributed random variables with zero mean and unit variance in $\mathbb{R}^2$.

B. Density Fields of Robots and Pollination Activity

In this section, we define the density fields of the microscopic model. During a deployment, when a *Flying* robot switches to

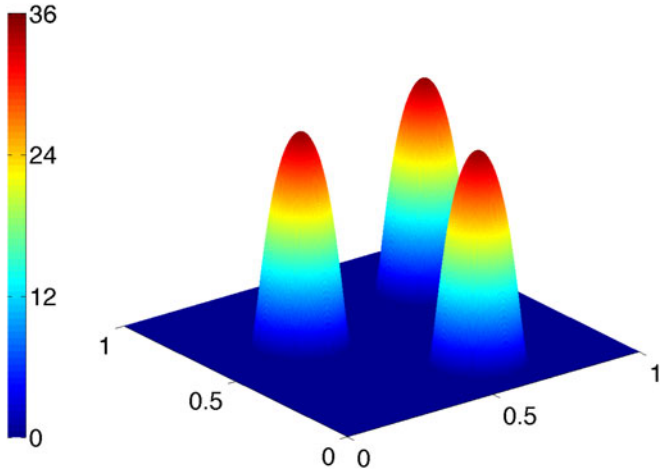

Fig. 2. Domain with three blob functions $G_\delta(\boldsymbol{x})$, where $\delta = 0.15$.

the *Hovering* state for pollination, it randomly selects a flower that it identifies within its sensing radius δ. In order to compute the density fields of robots and their pollination activity, we model the pdf of the location that the robot chooses to pollinate as a *blob function* $G_\delta(\boldsymbol{x})$. We define the blob function as

$$G_\delta(\boldsymbol{x}) = \begin{cases} \dfrac{C_g}{\delta^2} \exp\left(\dfrac{1}{|\boldsymbol{x}|^2/\delta^2 - 1}\right), & \text{if } |\boldsymbol{x}| < \delta \\ 0, & \text{otherwise} \end{cases} \tag{6}$$

where $C_g \approx 2.1436$ so that

$$\int_{\mathbb{R}^2} G_\delta(\boldsymbol{x}) d\boldsymbol{x} = 1.$$

G_δ satisfies the following properties:

1) $G_\delta \in C_0^\infty(\mathbb{R}^2)$, and its support is $\{\boldsymbol{x} : |\boldsymbol{x}| \le \delta\}$;
2) $\forall \boldsymbol{x}$, $|G_\delta(\boldsymbol{x})| \le C_g e^{-1} \delta^{-2} < \delta^{-2}$;
3) $\forall \boldsymbol{x}$, $|\partial_{x_i} G_\delta(\boldsymbol{x})| = \mathcal{O}(\delta^{-3})$ and $|\partial_{x_i x_j} G_\delta(\boldsymbol{x})| = \mathcal{O}(\delta^{-4})$, $i, j = 1, 2$.

Fig. 2 illustrates a domain with three blob functions, each with the same sensing radius parameter δ.

Remark IV.1: The blob function serves as a mean field approximation of pollination activity. That is, instead of modeling a robot's selection of a particular flower to pollinate, we consider the probability density of the robot's flower visits over multiple deployments, or alternatively, the flower visits by a large number of robots over a single deployment. Each crop row is modeled as a continuum of possible pollination locations, and thus, a robot can choose to hover at any position within the support of its corresponding blob function.

For all $\Sigma \subset \mathbb{R}^2$, we define the indicator function as

$$\mathbb{1}_\Sigma(\boldsymbol{x}) = \begin{cases} 1, & \text{if } \boldsymbol{x} \in \Sigma \\ 0, & \text{otherwise.} \end{cases}$$

We also define

$$\text{dis}(\boldsymbol{x}, \Sigma) := \inf\{|\boldsymbol{x} - \boldsymbol{y}| : \boldsymbol{y} \in \Sigma\}$$

$$\Sigma_{\text{in}}^\zeta := \{\boldsymbol{x} : \text{dis}(\boldsymbol{x}, \Sigma^c) \ge \zeta\} \tag{7}$$

$$\Sigma_{\text{out}}^\zeta := \{\boldsymbol{x} : \text{dis}(\boldsymbol{x}, \Sigma) \le \zeta\} \tag{8}$$

for some constant $\zeta > 0$, where Σ^c is the complement of Σ. From these definitions, Σ_{in}^ζ and $\Sigma_{\text{out}}^\zeta$ are obtained by shrinking and expanding, respectively, the boundary of Σ by a layer of width ζ. Hence, $\Sigma_{\text{in}}^\zeta \subset \Sigma \subset \Sigma_{\text{out}}^\zeta$.

Let $\boldsymbol{X}(t)$ be a stochastic process in $\mathbb{R}^2$ that satisfies the SDE (4). For all $t > s \ge 0$ and $\boldsymbol{x}, \boldsymbol{y} \in \mathbb{R}^2$, we denote the transition probability measure by $P(\Sigma, t|\boldsymbol{y}, s) = P(\boldsymbol{X}(t) \in \Sigma | \boldsymbol{X}(s) = \boldsymbol{y})$ and the transition pdf by $p_e(\boldsymbol{x}, t|\boldsymbol{y}, s)$. These functions satisfy

$$P(\Sigma, t|\boldsymbol{y}, s) = \int_\Sigma p_e(\boldsymbol{x}, t|\boldsymbol{y}, s) d\boldsymbol{x}$$

$$p_e(\boldsymbol{x}, t|\boldsymbol{y}, s) = \frac{1}{4\pi D(t-s)} \exp\left\{-\frac{|\boldsymbol{x} - \boldsymbol{y} - \int_s^t \boldsymbol{v}(\tau) d\tau|^2}{4D(t-s)}\right\}.$$

In our simulation of the microscopic model, we discretize the velocity $\boldsymbol{v}(t)$, and hence, the transition pdf from time t_m to time t_{m+1} is given by

$$p(\boldsymbol{x}, t_{m+1}|\boldsymbol{y}, t_m) = \frac{1}{4\pi D \Delta t} \exp\left\{-\frac{|\boldsymbol{x} - \boldsymbol{y} - \boldsymbol{v}(t_m)\Delta t|^2}{4D\Delta t}\right\}. \tag{9}$$

We now define the *actual density fields* of *Flying* robots and *Hovering* robots, respectively, at each location $\boldsymbol{x} \in \Omega$ and each time t_m as

$$\rho_1^\delta(\boldsymbol{x}, t_m) := \frac{1}{N} \sum_{i \in F_m} G_\delta(\boldsymbol{x} - \boldsymbol{X}_m^i) \tag{10}$$

$$\rho_2^\delta(\boldsymbol{x}, t_m) := \frac{1}{N} \sum_{j=1}^{n_f} \sum_{i \in H_{j,m}} G_\delta(\boldsymbol{x} - \boldsymbol{X}_m^i). \tag{11}$$

To confirm that these are robot density fields, note that

$$\int_\Sigma G_\delta(\boldsymbol{x} - \boldsymbol{X}_m^i) d\boldsymbol{x} \approx \mathbb{1}_\Sigma(\boldsymbol{X}_m^i).$$

The above identity strictly holds only when $\boldsymbol{X}_m^i \notin \Sigma_{\text{out}}^\delta - \Sigma_{\text{in}}^\delta$; otherwise, the range of the blob will exceed the boundary and will cause *coverage outflow*, an error introduced in Section VII. Hence

$$\int_\Sigma \rho_1^\delta(\boldsymbol{x}, t_m) d\boldsymbol{x} \approx \frac{1}{N} \sum_{i \in F_m} \mathbb{1}_\Sigma(\boldsymbol{X}_m^i) \tag{12}$$

$$\int_\Sigma \rho_2^\delta(\boldsymbol{x}, t_m) d\boldsymbol{x} \approx \frac{1}{N} \sum_{j=1}^{n_f} \sum_{i \in H_{j,m}} \mathbb{1}_\Sigma(\boldsymbol{X}_m^i) \tag{13}$$

which are the numbers of *Flying* and *Hovering* robots, respectively, that are in region Σ at time t_m, divided by N.

We also define the actual density fields of *Flying* and *Hovering* robots, respectively, that are present after robots execute state transitions according to reactions (2) but before they execute their motion controllers during the time step Δt:

$$\bar{\rho}_1^\delta(\boldsymbol{x}, t_m) := \frac{1}{N} \sum_{i \in F_{m+1}} G_\delta(\boldsymbol{x} - \boldsymbol{X}_m^i)$$

$$\bar{\rho}_2^\delta(\boldsymbol{x}, t_m) := \frac{1}{N} \sum_{j=1}^{n_f} \sum_{i \in H_{j,m+1}} G_\delta(\boldsymbol{x} - \boldsymbol{X}_m^i). \tag{14}$$

Note that by (3), the positions of *Hovering* robots is unchanged during the time step, and therefore

$$\bar{\rho}_2^{\delta}(\boldsymbol{x}, t_m) = \rho_2^{\delta}(\boldsymbol{x}, t_{m+1}). \tag{15}$$

We denote the density of robot state transitions from *Flying* to *Hovering* between times t_m and t_{m+1} as $\text{FTH}(\boldsymbol{x}, t_m)$, and the density of transitions from *Hovering* to *Flying* as $\text{HTF}(\boldsymbol{x}, t_m)$. These densities can be expressed as

$$\text{FTH}(\boldsymbol{x}, t_m) := \frac{1}{N} \sum_{j=1}^{n_f} \sum_{i \in F_m} I_{i,j,m} L_j(\boldsymbol{X}_m^i) G_\delta(\boldsymbol{x} - \boldsymbol{X}_m^i)$$

$$\text{HTF}(\boldsymbol{x}, t_m) := \frac{1}{N} \sum_{j=1}^{n_f} \sum_{i \in H_{j,m}} J_{i,j,m} G_\delta(\boldsymbol{x} - \boldsymbol{X}_m^i)$$

where $L_j(\boldsymbol{x}) = \mathbb{1}_{\Gamma_j}(\boldsymbol{x})$, and $I_{i,j,m}$ and $J_{i,j,m}$ are independent random variables with

$$P(I_{i,j,m} = 1) = \Delta t \cdot k_{j,m}, \quad P(I_{i,j,m} = 0) = 1 - \Delta t \cdot k_{j,m}$$
$$P(J_{i,j,m} = 1) = \Delta t \cdot k_f, \quad P(J_{i,j,m} = 0) = 1 - \Delta t \cdot k_f$$

with indices $i = 1, ..., N$, $j = 1, ..., n_f$, and $m = 1, ..., M$ and $k_{j,m} := k_j(t_m)$. According to the reaction network (2),

$$\bar{\rho}_1^{\delta}(\boldsymbol{x}, t_m) = \rho_1^{\delta}(\boldsymbol{x}, t_m) - \text{FTH}(\boldsymbol{x}, t_m) + \text{HTF}(\boldsymbol{x}, t_m)$$
$$\bar{\rho}_2^{\delta}(\boldsymbol{x}, t_m) = \rho_2^{\delta}(\boldsymbol{x}, t_m) + \text{FTH}(\boldsymbol{x}, t_m) - \text{HTF}(\boldsymbol{x}, t_m). \tag{16}$$

At each time t_m, the total number of state transitions from *Flying* to *Hovering* in the region Σ is given by

$$\int_{\Sigma} \text{FTH}(\boldsymbol{x}, t_m) d\boldsymbol{x} \approx \frac{1}{N} \sum_{j=1}^{n_f} \sum_{i \in F_m} I_{i,j,m} L_j(\boldsymbol{X}_m^i) \mathbb{1}_{\Sigma}(\boldsymbol{X}_m^i). \tag{17}$$

Since each transition from *Flying* to *Hovering* indicates a robot pollination visit, $\text{FTH}(\boldsymbol{x}, t_m)$ is also the *actual density field of pollination activity* at time t_m. Thus, the actual cumulative density field of pollination activity by the swarm from time 0 to time t_m is given by

$$\rho_3^{\delta}(\boldsymbol{x}, t_m) = \sum_{\tau=0}^{m-1} \text{FTH}(\boldsymbol{x}, t_\tau). \tag{18}$$

We define the tuple of actual density fields as

$$\boldsymbol{\rho}^{\delta}(\boldsymbol{x}, t_m) = \left(\rho_1^{\delta}(\boldsymbol{x}, t_m), \rho_2^{\delta}(\boldsymbol{x}, t_m), \rho_3^{\delta}(\boldsymbol{x}, t_m)\right). \tag{19}$$

The goal of our analysis is to compare ρ_3^{δ} to the expected density field of pollination, which is defined in the next section.

V. Macroscopic Model

A. Definition

The macroscopic model consists of a set of ADR PDEs that describe the time evolution of the expected spatial distribution of the swarm. The model presented here was first defined in [13] for a similar pollination scenario. The states of the macroscopic model are $\rho_1(\boldsymbol{x}, t)$, $\rho_2(\boldsymbol{x}, t)$, and $\rho_3(\boldsymbol{x}, t)$, the *expected density fields* of *Flying* robots, *Hovering* robots, and cumulative pollination from time 0 to t, respectively. Using the parameters $\boldsymbol{v}(t)$, $k_j(t), j = 1, 2, ..., n_f$, k_f, D, and L_j that are defined in the microscopic model, the macroscopic model is given by

$$\begin{cases} \frac{\partial \rho_1}{\partial t} = -\boldsymbol{v} \cdot \nabla \rho_1 + D\Delta\rho_1 - \sum_{j=1}^{n_f} k_j L_j \rho_1 + k_f \rho_2 \\ \frac{\partial \rho_2}{\partial t} = \sum_{i=1}^{n_f} k_j L_j \rho_1 - k_f \rho_2 \\ \frac{\partial \rho_3}{\partial t} = \sum_{i=1}^{n_f} k_j L_j \rho_1 \end{cases} \tag{20}$$

with initial conditions specifying that all robots start in the *Flying* state and are distributed according to a blob function centered at $\boldsymbol{X}_0$:

$$\rho_1(\boldsymbol{x}, 0) = G_\delta(\boldsymbol{x} - \boldsymbol{X}_0), \ \rho_2(\boldsymbol{x}, 0) = 0, \ \rho_3(\boldsymbol{x}, 0) = 0. \tag{21}$$

The initial conditions of the macroscopic model and microscopic model are consistent, i.e.,

$$\rho_i(\boldsymbol{x}, 0) = \rho_i^{\delta}(\boldsymbol{x}, 0), = 1, 2, 3. \tag{22}$$

We define the tuple of expected density fields as

$$\boldsymbol{\rho}(\boldsymbol{x}, t) = (\rho_1(\boldsymbol{x}, t), \rho_2(\boldsymbol{x}, t), \rho_3(\boldsymbol{x}, t)). \tag{23}$$

B. Numerical Solution

We use the operator splitting method to numerically solve the macroscopic model with the same time discretization as in (1). We define the following three operators:

$$\text{ADV}_m(\boldsymbol{\rho}) = (\ -\boldsymbol{v}(t_m) \cdot \nabla \rho_1, \ 0, \ 0\ )$$
$$\text{DIFF}(\boldsymbol{\rho}) = (\ D\Delta\rho_1, \ 0, \ 0\ )$$
$$\text{REACT}_m(\boldsymbol{\rho}) = \Big(k_f \rho_2 - \sum_{j=1}^{n_f} k_{j,m} L_j \rho_1, \sum_{j=1}^{n_f} k_{j,m} L_j \rho_1 - k_f \rho_2, \sum_{j=1}^{n_f} k_{j,m} L_j \rho_1 \Big). \tag{24}$$

We split the macroscopic model (20), (21) into three parts:

$$\frac{\partial \boldsymbol{\rho}}{\partial t} = \text{ADV}_m(\boldsymbol{\rho}) \tag{25}$$
$$\frac{\partial \boldsymbol{\rho}}{\partial t} = \text{DIFF}(\boldsymbol{\rho}) \tag{26}$$
$$\frac{\partial \boldsymbol{\rho}}{\partial t} = \text{REACT}_m(\boldsymbol{\rho}). \tag{27}$$

Denote the solution operators of (25)–(27) with respect to time step Δt by $H_1(\Delta t)$, $H_2(\Delta t)$, and $H_3(\Delta t)$, respectively. That is, $\boldsymbol{\rho}(\boldsymbol{x}, t_{m+1}) = H_1(\Delta t)\boldsymbol{\rho}(\boldsymbol{x}, t_m)$ if $\boldsymbol{\rho}(\boldsymbol{x}, t_{m+1})$ is the solution of (25) with initial condition $\boldsymbol{\rho}_0(\boldsymbol{x}) = \boldsymbol{\rho}(\boldsymbol{x}, t_m)$. Using these operators, we can compute the expected density fields at time t_{m+1} as

$$\boldsymbol{\rho}(\boldsymbol{x}, t_{m+1}) = H_1(\Delta t) H_2(\Delta t) H_3(\Delta t) \boldsymbol{\rho}(\boldsymbol{x}, t_m). \tag{28}$$

This is a first-order splitting method, i.e.,

$$\int_{\mathbb{R}^2} |\boldsymbol{\rho}_e(\boldsymbol{x}, T) - \boldsymbol{\rho}(\boldsymbol{x}, T)| d\boldsymbol{x} \ \leq \ C_\delta \Delta t \tag{29}$$

where $\boldsymbol{\rho}_e$ is the exact solution of model (20) and $\boldsymbol{\rho}$ is defined by (28). We note that C_δ depends on δ and that $\lim_{\delta \to 0} C_\delta = \infty$. We choose the values of Δt and δ based on the numerical simulation results in Section VIII to ensure that the above error is small.

We also define the expected density fields of *Flying* and *Hovering* robots that are present after the reactions but before robot motion during a time step

$$\bar{\rho}_i(\boldsymbol{x}, t_m) := H_3(\Delta t)\rho_i(\boldsymbol{x}, t_m),\ i = 1, 2 \tag{30}$$

which correspond to $\bar{\rho}_i^\delta(\boldsymbol{x}, t_m),\ i = 1, 2$, in the microscopic model. Equations (28) and (30) also yield

$$\rho_i(\boldsymbol{x}, t_{m+1}) = H_1(\Delta t)H_2(\Delta t)\bar{\rho}_i(\boldsymbol{x}, t_m),\ i = 1, 2. \tag{31}$$

From the definitions of $H_1(\Delta t)$ and $H_2(\Delta t)$, we have that

$$\rho_1(\boldsymbol{x}, t_{m+1}) = \int_{\mathbb{R}^2} \bar{\rho}_1(\boldsymbol{y}, t_m)p(\boldsymbol{x}, t_{m+1}|\boldsymbol{y}, t_m)\boldsymbol{dy} \tag{32}$$

$$\rho_2(\boldsymbol{x}, t_{m+1}) = \bar{\rho}_2(\boldsymbol{x}, t_m). \tag{33}$$

Equation (32) holds because the transition pdf $p(\boldsymbol{x}, t_{m+1}|\boldsymbol{y}, t_m)$ is also the Green's function of the advection-diffusion equation (see [25, Th. 2.1]).

We numerically solve the three operators over a square domain $\bar{\Omega}$ with Neumann boundary conditions. The domain is defined to be large enough to contain all the robots almost surely over the entire duration of the deployment. For the advection operator (25), we use the Lax–Friedrichs scheme. For the diffusion operator (26), we use the Crank–Nicolson scheme and apply the discrete cosine transform to solve it. Finally, we solve the reaction operator (27) using the forward Euler scheme.

VI. Optimal Control of Coverage Strategies

We briefly summarize the optimal control problem that is solved in our previous work [13]. We use this approach to compute the optimal robot velocity $\mathbf{v}(t) = [v_1(t)\ v_2(t)]^T$ and pollination rates $k_j(t), j = 1, ..., n_f$, that minimize the error between a target distribution ρ_Ω and the expected pollination field ρ_3 at a given time T. Note that the performance of the optimal control method is not the focus of this paper.

For an open subset $X \subseteq \mathbb{R}^2$, $L^2(X)$ refers to the space of real-valued square-integrable functions. The norm $\|\cdot\|_{L^2(X)}$ is defined as $\|f\|_{L^2(X)} = (\int_X |f(\boldsymbol{x})|^2 d\boldsymbol{x})^{1/2}$ for each $f \in L^2(X)$. The notation $\langle\cdot,\cdot\rangle_{L^2(X)}$ refers to the inner product on $L^2(X)$, defined as $\int_X f(\boldsymbol{x})g(\boldsymbol{x})d\boldsymbol{x}$ for each $f, g \in L^2(X)$. For a natural number m, $\|\cdot\|_{L^2(X)^m}$ and $\langle\cdot,\cdot\rangle_{L^2(X)^m}$ refer to the natural extension of the norm and inner product on the product space $L^2(X)^m$. The vector of control parameters is defined as

$$\boldsymbol{u} := (u_1, u_2, ..., u_{n_f+2})$$

where $u_1 = v_1, u_2 = v_2$, and $u_{j+2} = k_j$ for $j = 1, ..., n_f$. Then, the optimal control problem is the following:

$$\min_{(\boldsymbol{\rho},\boldsymbol{u})\in Y\times U_{ad}} J(\boldsymbol{\rho}, \boldsymbol{u}) = \frac{1}{2}\|\rho_3(\cdot, T) - \rho_\Omega\|^2_{L^2(\mathbb{R}^2)} + \frac{\lambda}{2}\|\boldsymbol{u}\|^2_{L^2(0,T)^\kappa},\ \kappa = n_f + 2 \tag{34}$$

subject to (20) and (21). Hence, this is a PDE-constrained optimization problem. Here, $Y = C([0, T], L^2(\mathbb{R}^2)^3)$ is the space of vector-valued continuous functions $f : [0, T] \to L^2(\mathbb{R}^2)^3$, and U_{ad} is the set of admissible control inputs given by

$$U_{\text{ad}} = \{\boldsymbol{u} \in L^2(0, T)^{n_f+2} : u_i^{\min} \le u_i(t) \le u_i^{\max} \ \forall t \in (0, T)\}$$

where $u_i^{\min}$ and $u_i^{\max}$ are real-valued scalars defining the lower and upper bounds on the control parameters. These bounds are determined by the physical limitations on the robots, such as their maximum velocity. The bounds on the pollination rates k_j, $j = 1, ..., n_f$, additionally depend on the time step Δt, according to the constraint $k_j(t)\Delta t \le 1$.

The necessary conditions for optimality are used to derive a gradient descent method for numerically computing the optimal robot control parameters. Appendix A gives details on the directional derivatives that are used in this method.

VII. L^1-Convergence Analysis

In this section, we present the main result of this paper: a rigorous convergence analysis to estimate the error between the expected density field $\boldsymbol{\rho}$ from the macroscopic model and the actual density field $\boldsymbol{\rho}^\delta$ from the microscopic model. Our result shows that the error depends on the number of robots N, the time discretization Δt, and the sensing radius δ.

In our analysis, we use the L^1 norm, which is the most natural norm for particle transportation, to quantify the degree of coverage by the swarm. This is because the L^1 norms of ρ_1^δ and ρ_2^δ directly measure the numbers of *Flying* robots and *Hovering* robots, respectively [see (12) and (13)], and the L^1 norm of ρ_3^δ measures the cumulative number of crop visits [see (17) and (18)], which is the metric of interest in the application. Note that in the optimal control method in Section VI, we use the L^2 norm in the objective function since it is convenient for optimal control. This is due to the inner-product structure of L^2 spaces, which makes them self-dual; L^1 function spaces lack this structure. Since our domain is a finite region, bounding the L^2 norm also bounds the L^1 norm according to the Cauchy–Schwarz inequality $\|\cdot\|_1 \le C\|\cdot\|_2$.

The error bound that we derive in this section consists of four components: the *time-discretization error*, the *coverage outflow*, the *coverage insufficiency,* and the *sampling error*. The time-discretization error arises from our time-splitting method. The coverage outflow happens at the boundary of the region of crop rows $\Gamma_j, j = 1, 2, ..., n_f$: if a robot is pollinating in a row Γ_j at a position that is very close to the boundary of Γ_j, then part of the corresponding blob may exceed Γ_j, which generates some loss of coverage. Coverage insufficiency arises when there are too few robots in the swarm to cover the entire field, given the size of δ, and can be improved by deploying more robots. The most significant error component is the sampling error, which arises from the stochasticity in the robot motion and task switching. The error bound indicates the existence of an optimal δ for a fixed swarm size, which we verify in simulation in Section VIII.

Let $\boldsymbol{\rho}^\delta(\boldsymbol{x}, t_m)$ and $\boldsymbol{\rho}(\boldsymbol{x}, t_m)$ be defined as in (19) and (28), respectively. We also define the L^1 norm of a function $f : \mathbb{R}^2 \times [0, T] \to \mathbb{R}$ and the error functions as follows:

$$\|f(\cdot, t)\|_{1,\Sigma} := \int_\Sigma |f(\boldsymbol{x}, t)|\boldsymbol{dx},\ \forall \Sigma \subset \mathbb{R}^2$$

$$e_i(\boldsymbol{x}, t_m) := \rho_i(\boldsymbol{x}, t_m) - \rho_i^\delta(\boldsymbol{x}, t_m),\quad i = 1, 2, 3$$

$$E_m := \max\{\|e_1(\cdot, t_m)\|_1, \|e_2(\cdot, t_m)\|_1\}.$$

Theorem VII.1: Assume that $\boldsymbol{v}(t) \in C^1([0, \infty])$, $D > 0$, and $k_i(t) \in C([0, \infty])$, $i = 1, ..., n_f$. Suppose that $\bar{\Omega} \subset \mathbb{R}^2$ is

a large enough square such that $\Omega \subset \bar{\Omega}$, and $\exists \zeta > 0$ such that

$$\boldsymbol{X}_m^i \in \bar{\Omega}_{\text{in}}^{2\zeta} \quad \forall m = 1, ..., M,\ i = 1, ..., N$$

almost surely, and $\delta < \zeta$, $\Delta t \ll \zeta$. We define $|\bar{\Omega}|$ as the area of $\bar{\Omega}$, C as an independent constant, Γ as $\cup_{j=1}^{n_f} \Gamma_j$, and $\Gamma_{\text{in}}^{\delta}$ and $\Gamma_{\text{out}}^{\delta}$ as in (7) and (8). We also set

$$K = k_f + \sum_{j=1}^{n_f} \max_{t\in[0,T]} k_j(t),$$

$$P_\delta = \max_m P\left(\boldsymbol{X}_m^i \in \Gamma_{\text{out}}^{\delta} - \Gamma_{\text{in}}^{\delta}\right) = \mathcal{O}(\delta).$$

Then, when N is sufficiently large, the following estimates are true with a probability greater than

$$1 - \frac{CT}{\Delta t} N^{\left[-\frac{1}{3}(\ln N)\Delta t^2 + 2\right]}. \tag{35}$$

(i) (Error in distributions of Hovering and Flying robots)

$$\|e_i(\cdot, t_m)\|_1 \le Ce^{KT}\left[\delta^{-4}\sqrt{D}|\bar{\Omega}|\frac{\ln N}{\sqrt{N}} + P_\delta + \Delta t\right],\ i = 1, 2 \tag{36}$$

uniformly in m.

(ii) (Error in distribution of cumulative pollination)

$$\|e_3(\cdot, t_m)\|_1 \le CKTe^{KT}\left[\delta^{-4}\sqrt{D}|\bar{\Omega}|\frac{\ln N}{\sqrt{N}} + P_\delta + \Delta t\right] \tag{37}$$

uniformly in m.

Remark VII.2: In the inequalities (36) and (37), the error terms are interpreted in the following way:

1) $\frac{\ln N}{\sqrt{N}}$: Sampling error;
2) δ^{-4}: Coverage insufficiency;
3) P_δ: Coverage outflow;
4) Δt: Time-discretization error.

The sampling error is the main source of error in this model, due to the significant stochasticity in the robot motion and state transitions. The time-discretization error arises from the diffusion of the blob functions outside of $\bar{\Omega}$ in the macroscopic PDE model. This error is not as significant as the other errors, since $\bar{\Omega}$ is chosen to be large enough to contain the entire swarm almost surely throughout the selected time span $[0, T]$.

Note that the task switching and the motion of the robots depend on each other, i.e., the motion depends on which state a robot is in, and the task switching depends on whether a robot is above a crop region. We formulate the *error of motion* as

$$\text{EM}(\boldsymbol{x}) = \int_{\mathbb{R}^2} \bar{\rho}_1^{\delta}(\boldsymbol{y}, t_m) p(\boldsymbol{x}, t_{m+1}|\boldsymbol{y}, t_m)\boldsymbol{dy} - \rho_1^{\delta}(\boldsymbol{x}, t_{m+1}). \tag{38}$$

The first term is the expected density of *Flying* robots at t_{m+1} based on the actual density that is present after the reaction at t_m, and the second term is the actual density at t_{m+1}. We also formulate the *error of reaction* as

$$\begin{aligned}\text{ER}(\boldsymbol{x}) \ &= -\Delta t \sum_{j=1}^{n_f} k_{j,m} L_j(\boldsymbol{x}) \rho_1^{\delta}(\boldsymbol{x}, t_m) + \text{FTH}(\boldsymbol{x}, t_m) \\ &\quad + \Delta t k_f \rho_2^{\delta}(\boldsymbol{x}, t_m) - \text{HTF}(\boldsymbol{x}, t_m).\end{aligned} \tag{39}$$

Here, $\text{FTH}(\boldsymbol{x}, t_m)$ and $\text{HTF}(\boldsymbol{x}, t_m)$ are the actual densities of robot state transitions between *Flying* and *Hovering*, whereas the other two terms are the expected densities of state transitions. To prove Theorem VII.1, we track the iteration of the error E_m over the time span $[0, T]$ using the following proposition.

Proposition VII.3 (Iteration of error): For all $m = 0, ..., M-1$, we have that

$$E_{m+1} \ \le \ (1 + \Delta tK)E_m + \|\text{ER}(\cdot)\|_1 + \|\text{EM}(\cdot)\|_1. \tag{40}$$

Proof of Proposition VII.3: We can decompose the error in the following way. First, using (32), we derive the inequality:

$$\begin{aligned}|e_1(\boldsymbol{x}, t_{m+1})| &= \ |\rho_1(\boldsymbol{x}, t_{m+1}) - \rho_1^{\delta}(\boldsymbol{x}, t_{m+1})| \\ &= \left|\int_{\mathbb{R}^2} \bar{\rho}_1(\boldsymbol{y}, t_m) p(\boldsymbol{x}, t_{m+1}|\boldsymbol{y}, t_m)\boldsymbol{dy} - \rho_1^{\delta}(\boldsymbol{x}, t_{m+1})\right| \\ &\le \left|\int_{\mathbb{R}^2} [\bar{\rho}_1(\boldsymbol{y}, t_m) - \bar{\rho}_1^{\delta}(\boldsymbol{y}, t_m)] p(\boldsymbol{x}, t_{m+1}|\boldsymbol{y}, t_m)\boldsymbol{dy}\right| \\ &\quad + \ |\text{EM}(\boldsymbol{x})|.\end{aligned} \tag{41}$$

Then, by taking the L^1 norm of both sides of (41), we obtain

$$\|e_1(\cdot, t_{m+1})\|_1 \le \|\bar{\rho}_1(\cdot, t_m) - \bar{\rho}_1^{\delta}(\cdot, t_m)\|_1 + \|\text{EM}(\cdot)\|_1. \tag{42}$$

For abbreviation, we omit $(\boldsymbol{x}, t_m)$. By (16) and the definition of $\text{ER}(\boldsymbol{x})$ in (39),

$$\begin{aligned}\|\bar{\rho}_1 - \bar{\rho}_1^{\delta}\|_1 \le \ &\left\|(\bar{\rho}_1 - \rho_1) - (\bar{\rho}_1^{\delta} - \rho_1^{\delta})\right\|_1 + \|\rho_1 - \rho_1^{\delta}\|_1 \\ \le \ &\left\|\text{FTH} - \Delta t \sum_{j=1}^{n_f} k_{j,m} L_j \rho_1 + \Delta t k_f \rho_2 - \text{HTF}\right\|_1 + E_m \\ \le \ &\left\|\Delta t \sum_{j=1}^{n_f} k_{j,m} L_j (\rho_1 - \rho_1^{\delta})\right\|_1 + \|\Delta t k_f (\rho_2 - \rho_2^{\delta})\|_1 \\ &+ \ \|\text{ER}(\cdot)\|_1 + E_m \\ \le \ &(1 + \Delta tK)E_m + \|\text{ER}(\cdot)\|_1.\end{aligned} \tag{43}$$

Now, we combine (42) and (43) to obtain

$$\|e_1(\cdot, t_{m+1})\|_1 \le (1 + \Delta tK)E_m + \|\text{ER}(\cdot)\|_1 + \|\text{EM}(\cdot)\|_1. \tag{44}$$

Similarly, by (15) and (33),

$$\begin{aligned}\|e_2(\cdot, t_{m+1})\|_1 &= \|\rho_2(\cdot, t_{m+1}) - \rho_2^{\delta}(\cdot, t_{m+1})\|_1 \\ &= \ \|\bar{\rho}_2(\cdot, t_m) - \bar{\rho}_2^{\delta}(\cdot, t_m)\|_1 \\ &\le \ \|(\bar{\rho}_2 - \rho_2) - (\bar{\rho}_2^{\delta} - \rho_2^{\delta})\|_1 + \|\rho_2 - \rho_2^{\delta}\|_1 \\ &\le \ (1 + \Delta tK)E_m + \|\text{ER}(\cdot)\|_1.\end{aligned} \tag{45}$$

Combining (44) and (45), we arrive at

$$E_{m+1} \le (1 + \Delta tK)E_m + \|\text{ER}(\cdot)\|_1 + \|\text{EM}(\cdot)\|_1.$$

■

In the remainder of this section, we will focus on estimating $\|\text{ER}(\cdot)\|_1$ and $\|\text{EM}(\cdot)\|_1$. To estimate the L^1 norm, we utilize a spatial discretization. Denote $\bar{\Omega}$ by $[a_0, a_f] \times [b_0, b_f]$, where

$b_f - b_0 = a_f - a_0 = \sqrt{|\bar{\Omega}|}$. Select a spatial resolution to be

$$h = \frac{\sqrt{|\bar{\Omega}|}}{\lceil \sqrt{N} \rceil} \tag{46}$$

and discretize $\bar{\Omega}$ into cells of size $h \times h$ as follows:

$$\bar{\Omega}_h = \{(a_0 + ih, b_0 + jh) \in \bar{\Omega} : 0 \le i, j < \lceil \sqrt{N} \rceil\}. \tag{47}$$

We note that there is no spatial discretization in the simulation of the microscopic model, but the selection of h matters in the analysis. The choice of h involves a tradeoff: smaller h yields a more accurate estimate, while larger h provides a higher probability that the estimate is true. By (46), there are $\lceil \sqrt{N} \rceil^2$ cells in all, and hence, each cell contains one robot on average. For $\boldsymbol{F}(\boldsymbol{x}) : \mathbb{R}^2 \to \mathbb{R}^2 = (f_1(\boldsymbol{x}), f_2(\boldsymbol{x}))$, we introduce the infinity norm

$$\|\boldsymbol{F}(\cdot)\|_\infty := \sup\{|f_1(\boldsymbol{x})|, |f_2(\boldsymbol{x})| : \boldsymbol{x} \in \mathbb{R}^2\}.$$

Then, we have the following quadrature error.

Lemma VII.4 (Quadrature error): Suppose that $f \in C^\infty(\mathbb{R}^2)$. Then, the following inequality holds:

$$\left| \|f(\cdot)\|_{1,\bar{\Omega}} - \sum_{\boldsymbol{\alpha} \in \bar{\Omega}_h} |f(\boldsymbol{\alpha})| h^2 \right| \le 2|\bar{\Omega}| \|\nabla f(\cdot)\|_\infty h.$$

The proof of Lemma VII.4 is based on the mean value theorem. A similar estimate can be found in [21, Lemma 6.2]. In the rest of this paper, we always assume that N is sufficiently large for our estimates.

Claim VII.5 (Error of motion): There exists an independent constant, C, such that

$$\|\mathrm{EM}(\cdot)\|_1 \le C\Delta t |\bar{\Omega}| \sqrt{D} \delta^{-4} \frac{\ln N}{\sqrt{N}} + \Delta t^2$$

with probability greater than $1 - N^{\left[-\frac{1}{3}(\ln N)\Delta t^2 + 2\right]}$.

Proof of Claim VII.5: We note that

$$\|\mathrm{EM}(\cdot)\|_1 = \|\mathrm{EM}(\cdot)\|_{1,\bar{\Omega}} + \|\mathrm{EM}(\cdot)\|_{1,\bar{\Omega}^c}.$$

First, we estimate $\|\mathrm{EM}(\cdot)\|_{1,\bar{\Omega}}$. We define the error of motion for the ith robot:

$$\begin{aligned} Y_i(\boldsymbol{x}) : \; &= \frac{1}{N} \int_{\mathbb{R}^2} G_\delta(\boldsymbol{y} - \boldsymbol{X}^i_m) p(\boldsymbol{x}, t_{m+1} | \boldsymbol{y}, t_m) d\boldsymbol{y} \\ &\quad - \frac{1}{N} G_\delta(\boldsymbol{x} - \boldsymbol{X}^i_{m+1}) \quad \text{if } i \in F_{m+1} \end{aligned} \tag{48}$$

and $Y_i(\boldsymbol{x}) = 0$ if $i \in \cup_j H_{j,m+1}$. Then, by (10), (14), and the definition of $\mathrm{EM}(\boldsymbol{x})$ in (38), we have

$$\mathrm{EM}(\boldsymbol{x}) = \sum_{i=1}^N Y_i(\boldsymbol{x}).$$

Note that the robots are independent of one another, and thus, $Y_i(\boldsymbol{x})$, $i = 1, ..., N$, are independent random variables for any fixed $\boldsymbol{x}$. These random variables have zero mean, i.e.,

$$E(Y_i(\boldsymbol{x})) = 0. \tag{49}$$

The proof of (49) is given in Appendix A, Claim B.1.

Now, we apply Bennett's inequality to obtain an upper bound for $|\mathrm{EM}(\boldsymbol{x})|$.

Lemma VII.6: (Bennett's inequality) Let Y_i be independent bounded random variables with $E(Y_i) = 0, Var(Y_i) = \sigma_i^2$, and $|Y_i| \le M_0$. Let $S = \sum_i Y_i$ and $V \ge \sum_i \sigma_i^2$. Then, for $\eta > 0$,

$$P\{|S| \ge \eta\} \le 2 \exp\left[-\frac{1}{2} \eta^2 V^{-1} B(M_0 \eta V^{-1}) \right] \tag{50}$$

where $B(\lambda) = 2\lambda^{-2}[(1+\lambda)\ln(1+\lambda) - \lambda]$, $\lambda > 0$, $\lim_{\lambda \to 0^+} B(\lambda) = 1$, and $B(\lambda) \sim 2\lambda^{-1} \ln \lambda$ as $\lambda \to \infty$.

The proof of Lemma VII.6 can be found in [4] and [18]. A direct computation yields

$$|Y_i(\boldsymbol{x})| \le \frac{1}{N\delta^2}, \quad \sum_{i=1}^N \mathrm{Var}(Y_i(\boldsymbol{x})) \le \frac{1}{N\delta^4}.$$

We set $\eta = \frac{\Delta t \ln N}{\sqrt{N}\delta^2}$, $M_0 = N^{-1}\delta^{-2}$, and $V = N^{-1}\delta^{-4}$ in Bennett's inequality to obtain the following estimate:

$$\begin{aligned} &P\left(|\mathrm{EM}(\boldsymbol{x})| \ge \Delta t \frac{\ln N}{\sqrt{N}\delta^2} \right) \\ &\le 2 \exp\left[-\frac{1}{2} \eta^2 V^{-1} B(M_0 \eta V^{-1}) \right] \\ &= 2 \exp\left[-\frac{1}{2} (\ln N)^2 \Delta t^2 B\left(\Delta t \frac{\ln N}{\sqrt{N}} \right) \right] \\ &\le 2 \exp\left[-\frac{1}{3} (\ln N)^2 \Delta t^2 \right] = 2N^{-\frac{1}{3}(\ln N)\Delta t^2} \end{aligned} \tag{51}$$

where we used the fact that $B\left(\Delta t \frac{\ln N}{\sqrt{N}}\right) \ge \frac{2}{3}$ when N is sufficiently large. Hence, we have

$$\sum_{\boldsymbol{\alpha} \in \bar{\Omega}_h} |\mathrm{EM}(\boldsymbol{\alpha})| h^2 \le \Delta t |\bar{\Omega}| \frac{\ln N}{\sqrt{N}\delta^2} \tag{52}$$

with probability greater than $1 - 2N^{\left[-\frac{1}{3}(\ln N)\Delta t^2 + 2\right]}$. Next, by Lemma VII.4,

$$\begin{aligned} &\left| \|\mathrm{EM}(\cdot)\|_{1,\bar{\Omega}} - \sum_{\boldsymbol{\alpha} \in \bar{\Omega}_h} |\mathrm{EM}(\boldsymbol{\alpha})| h^2 \right| \\ &\le 2|\bar{\Omega}| \|\nabla \mathrm{EM}(\cdot)\|_\infty h \le 2|\bar{\Omega}| \sum_{i=1}^N \|\nabla Y_i(\cdot)\|_\infty h. \end{aligned} \tag{53}$$

We claim that for each $i = 1, ..., N$,

$$\|\nabla Y_i(\cdot)\|_\infty \le \frac{C_2}{N} \sqrt{D} \Delta t \delta^{-4} \ln N \tag{54}$$

with probability greater than $1 - \exp\left[-\frac{1}{2}\Delta t (\ln N)^2\right]$, where C_2 is an independent constant. The proof of this claim is given in Appendix A, Claim B.2.

Combining inequalities (52)–(54), and plugging in the choice of h given by (46), we obtain

$$\begin{aligned} \|\mathrm{EM}(\cdot)\|_{1,\bar{\Omega}} &\le \Delta t \delta^{-2} |\bar{\Omega}| \frac{\ln N}{\sqrt{N}} + C_2 |\bar{\Omega}|^{3/2} \sqrt{D} \Delta t \delta^{-4} \frac{\ln N}{\sqrt{N}} \\ &\le C \Delta t |\bar{\Omega}| \sqrt{D} \delta^{-4} \frac{\ln N}{\sqrt{N}} \end{aligned} \tag{55}$$

with probability greater than $1 - 2N^{\left[-\frac{1}{3}(\ln N)\Delta t^2 + 2\right]}$, where C is an independent constant.

Next, we consider $\|\text{EM}(\cdot)\|_{1,\bar{\Omega}^c}$. This error is caused by diffusion: in the macroscopic model, the density of *Flying* robots diffuses immediately to the entire $\mathbb{R}^2$, whereas in the microscopic model, the actual density of *Flying* robots always stays in $\bar{\Omega}$.

We claim that

$$\|\text{EM}(\cdot)\|_{1,\bar{\Omega}^c} \;\le\; \Delta t^2. \tag{56}$$

The proof of this claim is given in Appendix A, Claim B.3. Now, we combine (55) and (56) to obtain

$$\|\text{EM}(\cdot)\|_1 \;\le\; C\Delta t|\bar{\Omega}|\sqrt{D}\delta^{-4}\frac{\ln N}{\sqrt{N}} + \Delta t^2$$

with probability greater than $1 - N^{\left[-\frac{1}{3}(\ln N)\Delta t^2+2\right]}$. This completes the proof of Claim VII.5. ■

Claim VII.7 (Error of reaction): There exists an independent constant, C, such that

$$\|\text{ER}(\cdot)\|_1 \;\le\; CK\Delta t\delta^{-3}|\bar{\Omega}|\frac{\ln N}{\sqrt{N}} \;+\; \Delta tKP_\delta$$

with probability greater than $1 - CN^{\left[-\frac{1}{3K}(\ln N)\Delta t+2\right]}$.

Proof of Claim VII.7: Define an intermediate term

$$\text{FTH}'(\boldsymbol{x},t_m) := \frac{1}{N}\sum_{j=1}^{n_f}\sum_{i\in F_m}\Delta t k_{j,m}L_j(\boldsymbol{X}^i_m)G_\delta(\boldsymbol{x}-\boldsymbol{X}^i_m).$$

Omitting $(\boldsymbol{x},t_m)$, we have

$$\begin{aligned}
&|\text{ER}(\boldsymbol{x})|\\
&= \left|-\Delta t\sum_{j=1}^{n_f}k_{j,m}L_j(\boldsymbol{x})\rho_1^\delta + \Delta t k_f\rho_2^\delta + \text{FTH} - \text{HTF}\right|\\
&\le |\text{SE}(\boldsymbol{x})| + |\text{OF}(\boldsymbol{x})|
\end{aligned}$$

where

$$\text{SE}(\boldsymbol{x}) = \left[(\text{FTH}-\text{FTH}') + (\Delta t k_f\rho_2^\delta - \text{HTF})\right](\boldsymbol{x},t_m)$$

$$\text{OF}(\boldsymbol{x}) = \left(\Delta t\sum_{j=1}^{n_f}k_{j,m}L_j(\boldsymbol{x})\rho_1^\delta - \text{FTH}'\right)(\boldsymbol{x},t_m).$$

Notably, FTH and FTH′ are supported in $\Gamma^\delta_{\text{out}}$, while $k_{j,m}L_j(\boldsymbol{x})\rho_1^\delta$ is supported in Γ. Therefore, OF($\boldsymbol{x}$) measures the *coverage outflow* at the boundary of Γ. FTH and HTF are the actual densities of robot state transitions between *Flying* and *Hovering*, whereas FTH′ and $\Delta t k_f\rho_2^\delta$ are the expected densities of these state transitions; therefore, SE($\boldsymbol{x}$) measures the *sampling error* of reaction.

First, we estimate $\|\text{OF}(\cdot)\|_1$. We define $L(\boldsymbol{x}) = \mathbb{1}_\Gamma(\boldsymbol{x})$. Note that by the definitions of $L_j(\boldsymbol{x})$ and $L(\boldsymbol{x})$, we have that

$$L(\boldsymbol{x}) = \sum_{j=1}^{n_f}L_j(\boldsymbol{x}).$$

Now, using the definition of ρ_1^δ from (10), we obtain

$$\text{OF}(\boldsymbol{x}) = \frac{\Delta t}{N}\sum_{i\in F_m}\sum_{j=1}^{n_f}k_{j,m}\left(L_j(\boldsymbol{x}) - L_j(\boldsymbol{X}^i_m)\right)G_\delta(\boldsymbol{x}-\boldsymbol{X}^i_m).$$

Let us define

$$Z_i := \begin{cases}\frac{1}{N}\sum_{j=1}^{n_f}k_{j,m}\|(L_j(\cdot)-L_j(\boldsymbol{X}^i_m))G_\delta(\cdot-\boldsymbol{X}^i_m)\|_1, & \text{if } i\in F_m\\ 0, & \text{if } i\in\cup_{j=1}^{n_f}H_{j,m}\end{cases}$$

and

$$Z_i' := Z_i - E(Z_i).$$

Then, Z_i is coverage outflow of each individual robot, and

$$\|\text{OF}(\cdot)\|_1 \le\; \Delta t\sum_{i=1}^{N}Z_i = \Delta t\sum_{i=1}^{N}\left(Z_i' + E(Z_i)\right). \tag{57}$$

From the fact that $G_\delta(\boldsymbol{x})$ is supported in $\{\boldsymbol{x}:|\boldsymbol{x}|\le\delta\}$, it is straightforward to see that $(L_j(\boldsymbol{x}) - L_j(\boldsymbol{X}^i_m))G_\delta(\boldsymbol{x}-\boldsymbol{X}^i_m)\equiv 0$ if $\boldsymbol{X}^i_m\notin\Gamma^\delta_{\text{out}}-\Gamma^\delta_{\text{in}}$. When $\boldsymbol{X}^i_m\in\Gamma^\delta_{\text{out}}-\Gamma^\delta_{\text{in}}$, we have

$$\begin{aligned}
Z_i \;&\le\; \frac{K}{N}\int_{\mathbb{R}^2}|(L(\boldsymbol{x})-L(\boldsymbol{X}^i_m))G_\delta(\boldsymbol{x}-\boldsymbol{X}^i_m)|d\boldsymbol{x}\\
&\le\; \frac{1}{N}\int_{\mathbb{R}^2}G_\delta(\boldsymbol{x}-\boldsymbol{X}^i_m)d\boldsymbol{x} \;=\; \frac{K}{N}.
\end{aligned}$$

Hence

$$E(Z_i) \;\le\; \frac{K}{N}P\left\{\boldsymbol{X}^i_m\in\Gamma^\delta_{\text{out}}-\Gamma^\delta_{\text{in}}\right\} \;\le\; \frac{K}{N}P_\delta. \tag{58}$$

Note that Z_i' are independent and identically distributed random variables with $E(Z_i')=0$, so we can apply Bennett's inequality (see Lemma VII.6) again to estimate $|\sum_i Z_i'|$. We set $\eta = K\ln N/\sqrt{N}$ and compute M_0 and V as follows: $|Z_i'|\le K/N =: M_0$ and $\sum_i Var(Z_i')\le NM_0^2 = K^2/N =: V$. Plugging η, M_0, and V into Bennett's inequality, we arrive at

$$P\left(\left|\sum_{i=1}^{N}Z_i'\right| \;\ge\; \frac{K\ln N}{\sqrt{N}}\right) \;\le\; 2\exp\left[-\frac{(\ln N)^2}{3}\right]. \tag{59}$$

Combining (57)–(59), we obtain

$$\|\text{OF}(\cdot)\|_1 \;\le\; \Delta tK\frac{\ln N}{\sqrt{N}} + \Delta tKP_\delta \tag{60}$$

with probability greater than $1-2\exp\left[-\frac{1}{3}(\ln N)^2\right]$.

Next, we estimate $\|\text{SE}(\cdot)\|_1$. Since SE($\boldsymbol{x}$) is supported in $\bar{\Omega}$, we have that $\|\text{SE}(\cdot)\|_1 = \|\text{SE}(\cdot)\|_{1,\bar{\Omega}}$. We define

$$W_i(\boldsymbol{x}) := \varphi_i G_\delta(\boldsymbol{x}-\boldsymbol{X}^i_m), \quad i=1,...,N$$

where

$$\varphi_i := \begin{cases}\dfrac{1}{N}\displaystyle\sum_{j=1}^{n_f}(\Delta t k_{j,m} - I_{i,j,m})L_j(\boldsymbol{X}^i_m), & \text{if } i\in F_m\\[2ex] \dfrac{1}{N}(J_{i,j,m} - \Delta t k_f), & \text{if } i\in H_{j,m}.\end{cases}$$

It can be verified that for a fixed $\boldsymbol{x}$, the random variables $W_i(\boldsymbol{x})$, $i = 1, ..., N$, are independent, and

$$\begin{aligned}
&\mathrm{SE}(\boldsymbol{x}) = \sum_{i=1}^{N} W_i(\boldsymbol{x}), \;\; E(W_i(\boldsymbol{x})) = 0 \\
&|W_i(\boldsymbol{x})| \leq \frac{1}{N\delta^2} \;\text{ and }\; |\mathrm{SE}(\boldsymbol{x})| \leq \frac{1}{\delta^2} \\
&\mathrm{Var}(W_i(\boldsymbol{x})) \;\leq\; \delta^{-4}\mathrm{Var}(\varphi_i) \;\leq\; \frac{\Delta t K}{N^2\delta^4}.
\end{aligned}$$

Using the estimate of quadrature error (see Lemma VII.4),

$$\begin{aligned}
&\left| \|\mathrm{SE}(\cdot)\|_{1,\bar{\Omega}} - \sum_{\boldsymbol{\alpha}\in\bar{\Omega}_h} |\mathrm{SE}(\boldsymbol{\alpha})|h^2 \right| \;\leq\; 2|\bar{\Omega}|\|\nabla \mathrm{SE}(\cdot)\|_\infty h \\
&\leq\; 2|\bar{\Omega}| \sum_{i=1}^{N} |\varphi_i| \|\nabla G_\delta(\cdot - \boldsymbol{X}_m^i)\|_\infty h \;\leq\; 5|\bar{\Omega}|\delta^{-3} \sum_{i=1}^{N} |\varphi_i| h.
\end{aligned} \tag{61}$$

Next, we claim that

$$\sum_{i=1}^{N} |\varphi_i| \;\leq\; 2\Delta t K \tag{62}$$

with probability greater than $1 - 2\exp\left[-C_1 \Delta t K N/2\right]$, where C_1 is an independent constant. The proof of this claim is given in Appendix A, Claim B.4. Now, we apply Bennett's inequality again to estimate $\mathrm{SE}(\boldsymbol{\alpha})$. Setting $\eta = \Delta t \frac{\ln N}{\sqrt{N}\delta^2}$, $M_0 = \frac{1}{N\delta^2}$, $V = \frac{\Delta t K}{N\delta^4}$ and plugging these parameters into (50), we obtain

$$P\left(|\mathrm{SE}(\boldsymbol{\alpha})| \;\geq\; \Delta t \frac{\ln N}{\sqrt{N}\delta^2} \right) \;\leq\; 2N^{\left[-\frac{1}{3K}(\ln N)\Delta t\right]}$$

Hence,

$$\begin{aligned}
&P\left(\sum_{\boldsymbol{\alpha}\in\bar{\Omega}_h} |\mathrm{SE}(\boldsymbol{\alpha})|h^2 \;\leq\; \Delta t \delta^{-2}|\bar{\Omega}| \frac{\ln N}{\sqrt{N}} \right) \\
&\geq\; 1 - 2N^{\left[-\frac{1}{3K}(\ln N)\Delta t + 2\right]}.
\end{aligned} \tag{63}$$

Combining (61)–(63), and noting that $\exp(-N) \ll N^{-(\ln N)\Delta t + 2}$, we find that

$$\begin{aligned}
\|\mathrm{SE}(\cdot)\|_1 \;&\leq\; 10\Delta t \delta^{-3} K \frac{|\bar{\Omega}|^{3/2}}{\sqrt{N}} + \Delta t |\bar{\Omega}| \delta^{-2} \frac{\ln N}{\sqrt{N}} \\
&\leq\; C_2 \Delta t K \delta^{-3} |\bar{\Omega}| \frac{\ln N}{\sqrt{N}}
\end{aligned} \tag{64}$$

with probability greater than $1 - C_3 N^{\left[-\frac{1}{3K}(\ln N)\Delta t + 2\right]}$, where C_2 and C_3 are independent constants. Finally, by combining (60) and (64), we conclude that

$$\|\mathrm{ER}(\cdot)\|_1 \;\leq\; \mathrm{CK}\Delta t \delta^{-3} |\bar{\Omega}| \frac{\ln N}{\sqrt{N}} \;+\; \Delta t K P_\delta$$

with probability greater than $1 - \mathrm{CN}^{\left[-\frac{1}{3K}(\ln N)\Delta t + 2\right]}$, which completes the proof of Claim VII.7. ■

We now show how Theorem VII.1 follows from Proposition VII.3, Claim VII.5, and Claim VII.7.

Proof of Theorem VII.1: Set $\beta = 1 + K\Delta t$. By combining the inequalities in Proposition VII.3, Claim VII.5, and Claim VII.7, we find that

$$E_{m+1} \;\leq\; \beta E_m + C' K \left[\Delta t \delta^{-4} \sqrt{D} |\bar{\Omega}| \frac{\ln N}{\sqrt{N}} + \Delta t P_\delta + \Delta t^2 \right] \tag{65}$$

with probability greater than $1 - C' N^{\left[-\frac{1}{3}(\ln N)\Delta t^2 + 2\right]}$, where C' is an independent constant. Note that $E_0 = 0$. Iterating over m by using (65), we obtain

$$\begin{aligned}
E_{m+1} \;&\leq\; C' K \Delta t \frac{\beta^{m+1} - 1}{\beta - 1} \left[\delta^{-4} \sqrt{D} |\bar{\Omega}| \frac{\ln N}{\sqrt{N}} + P_\delta + \Delta t \right] \\
&\leq\; C' e^{KT} \left[\delta^{-4} \sqrt{D} |\bar{\Omega}| \frac{\ln N}{\sqrt{N}} + P_\delta + \Delta t \right]
\end{aligned}$$

uniformly in m with probability greater than

$$1 - \frac{C'T}{\Delta t} N^{\left[-\frac{1}{3}(\ln N)\Delta t^2 + 2\right]}. \tag{66}$$

Replacing C' with C, this proves part (i) of the theorem.

To prove part (ii), we start with the following inequality:

$$\begin{aligned}
&\|\rho_3(\cdot, t_m) - \rho_3^\delta(\cdot, t_m)\|_1 \\
&= \left\| \sum_{\tau=0}^{m-1} \sum_{j=1}^{n_f} k_{j,\tau} \Delta t L_j(\cdot) \rho_1(\cdot, t_\tau) - \sum_{\tau=0}^{m-1} \mathrm{FTH}(\cdot, t_\tau) \right\|_1 \\
&\leq\; \Delta t \left\| \sum_{\tau=0}^{m-1} \sum_{j=1}^{n_f} k_{j,\tau} L_j(\cdot) (\rho_1(\cdot, t_\tau) - \rho_1^\delta(\cdot, t_\tau)) \right\|_1 \\
&\quad + \left\| \sum_{\tau=0}^{m-1} \sum_{j=1}^{n_f} \Delta t k_{j,\tau} L_j(\cdot) \rho_1^\delta(\cdot, t_\tau) - \sum_{\tau=0}^{m-1} \mathrm{FTH}(\cdot, t_\tau) \right\|_1 \\
&=\; \Lambda_1 + \Lambda_2.
\end{aligned}$$

Here, Λ_1 is the cumulative error in the positions of the *Flying* robots, and Λ_2 is the cumulative error in reactions. We have that

$$\begin{aligned}
\Lambda_1 &\leq \Delta t K \sum_{\tau=0}^{m-1} E_\tau \\
&\leq\; \Delta t K \sum_{\tau=0}^{m-1} C' e^{KT} \left[\delta^{-4} \sqrt{D} |\bar{\Omega}| \frac{\ln N}{\sqrt{N}} + P_\delta + \Delta t \right] \\
&=\; C' T K e^{KT} \left[\delta^{-4} \sqrt{D} |\bar{\Omega}| \frac{\ln N}{\sqrt{N}} + P_\delta + \Delta t \right].
\end{aligned} \tag{67}$$

Next, we estimate Λ_2. We have

$$\Lambda_2 \;\leq\; \sum_{\tau=0}^{m-1} \left\| \sum_{i=1}^{n_f} \Delta t k_{j,\tau} L_j(\cdot) \rho_1^\delta - \mathrm{FTH}(\cdot, t_\tau) \right\|_1.$$

We note that the term $\sum_{i=1}^{n_f} \Delta t k_{j,\tau} L_j(\boldsymbol{x}) \rho_1^\delta - \mathrm{FTH}(\boldsymbol{x}, t_\tau)$ comprises part of the error of reaction $\mathrm{ER}(\boldsymbol{x})$, according to (39). Using an argument similar to the one in Claim VII.7, we

obtain

$$\Lambda_2 \;\le\; \sum_{\tau=0}^{m-1}\left[\mathrm{CK}\Delta t\delta^{-3}|\bar{\Omega}|\frac{\ln N}{\sqrt{N}} \;+\; \Delta t K P_\delta\right]$$
$$= T\left[\mathrm{CK}\delta^{-3}|\bar{\Omega}|\frac{\ln N}{\sqrt{N}} \;+\; K P_\delta\right]. \tag{68}$$

Combining (67) and (68), we arrive at our conclusion:

$$\|e_3(\cdot,t_m)\|_1 \;\le\; C'' K T e^{KT}\left[\delta^{-4}\sqrt{D}|\bar{\Omega}|\frac{\ln N}{\sqrt{N}} + P_\delta + \Delta t\right]$$

uniformly in m with probability greater than expression (66). Replacing C'' with C, this completes the proof of Theorem VII.1. ■

Thus far, we have presented an estimate of the L^1 error between the expected density field ρ_3 and the actual density field ρ_3^δ. We can compute the relative error between these density fields as

$$\mathrm{REL} = \frac{\|\rho_3(\cdot,T) - \rho_3^\delta(\cdot,T)\|_1}{\|\rho_3(\cdot,T)\|_1}. \tag{69}$$

In practice, however, we would want to compare ρ_3^δ to the *target distribution* ρ_Ω. Moreover, since the user will be satisfied as long as the crops are sufficiently pollinated, we can consider the overpollinated portion as an inefficiency rather than an error. Hence, we only count insufficient pollination as error. We define the *discrepancy* γ and *efficiency* as

$$\gamma = \frac{\|\rho_3^\delta(\cdot,T)\wedge\rho_\Omega(\cdot) - \rho_\Omega(\cdot)\|_1}{\|\rho_\Omega(\cdot)\|_1} \tag{70}$$

$$\text{Efficiency} = \frac{\|\rho_3^\delta(\cdot,T)\wedge\rho_\Omega(\cdot)\|_1}{\|\rho_3^\delta(\cdot,T)\|_1} \tag{71}$$

where $\rho_3^\delta(\boldsymbol{x},T)\wedge\rho_\Omega(\boldsymbol{x}) = \min\{\rho_3^\delta(\boldsymbol{x},T),\rho_\Omega(\boldsymbol{x})\}$. We also define the *intrinsic discrepancy*, which does not depend on N and δ, as

$$\gamma_\Omega = \frac{\|\rho_3(\cdot,T)\wedge\rho_\Omega(\cdot) - \rho_\Omega(\cdot)\|_1}{\|\rho_\Omega(\cdot)\|_1}. \tag{72}$$

Note that we do not analyze the error between the target distribution and the macroscopic model in this paper, since the optimal control is already studied in [13]. Given a *desired discrepancy* γ_d, our goal is to select N and δ such that

$$\gamma \;\le\; \gamma_d. \tag{73}$$

Toward this end, we present the following corollary.

Corollary VII.8: Under the same assumptions as in Theorem VII.1, we have that

$$\gamma \;\le\; \gamma_\Omega + C_4\left(\delta + \Delta t + (1+\delta^{-4})\frac{\ln N}{\sqrt{N}}\right) \tag{74}$$

with probability greater than $1 - \frac{CT}{\Delta t}N^{\left[-\frac{1}{3}(\ln N)\Delta t^2+2\right]}$. Here, C_4 is a constant that depends on $k_j(t)$, D, Γ_j, T, and $\bar{\Omega}$.

Proof: Since $|\min\{a,c\} - \min\{b,c\}| \le |a-b|$,

$$\|\rho_3^\delta\wedge\rho_\Omega(\cdot,T) - \rho_\Omega(\cdot)\|_1 \le \|\rho_3\wedge\rho_\Omega(\cdot,T) - \rho_\Omega(\cdot)\|_1$$
$$+\; \|\rho_3^\delta\wedge\rho_\Omega(\cdot,T) - \rho_3\wedge\rho_\Omega(\cdot,T)\|_1$$
$$\le\; \|\rho_3\wedge\rho_\Omega(\cdot,T) - \rho_\Omega(\cdot)\|_1 + \|\rho_3^\delta(\cdot,T) - \rho_3(\cdot,T)\|_1.$$

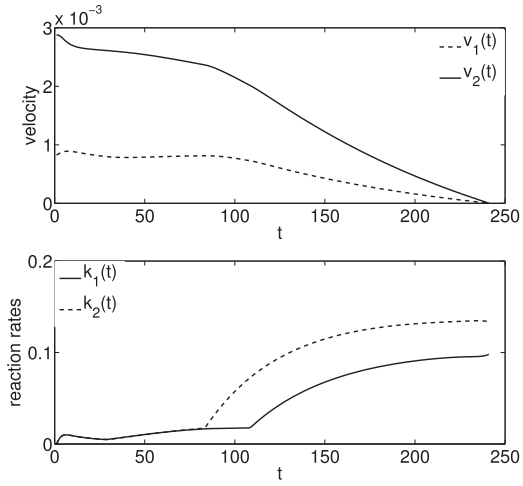

Fig. 3. *Top*: Robot velocity field $\boldsymbol{v}(t) = (v_1(t), v_2(t))$. *Bottom*: Robot pollination rates $k_1(t)$ and $k_2(t)$.

Hence

$$\gamma \;\le\; \gamma_\Omega + \frac{\|\rho_3^\delta(\cdot,T) - \rho_3(\cdot,T)\|_1}{\|\rho_\Omega(\cdot)\|_1}.$$

By Theorem VII.1, $\exists$ an independent constant $C_4' > 0$ such that

$$\|\rho_3^\delta(\cdot,T) - \rho_3(\cdot,T)\|_1 \;\le\; C_4'\left(\delta + \Delta t + (1+\delta^{-4})\frac{\ln N}{\sqrt{N}}\right).$$

Divide both sides by $\|\rho_\Omega(\cdot)\|_1$ and apply it to the previous inequality, and (74) is proved. ■

VIII. Simulation Results

In this section, we illustrate the design procedure in Section III for a simulated crop pollination scenario. Simulation results beyond those required for the design procedure are also presented to validate our convergence analysis.

1) *Set the parameter values.* We set the example crop field to be a unit square, $\Omega = [0,1]^2$, which has five rows of $n_f = 2$ different types of crops. The regions of type 1 crops and type 2 crops are defined, respectively, as $\Gamma_1 = \{(x_1,x_2) : x_1 \in [0.05,0.15]\cup[0.45,0.55]\cup[0.85,0.95], x_2 \in [0.05,0.95]\}$ and $\Gamma_2 = \{(x_1,x_2) : x_1 \in [0.25,0.35]\cup[0.65,0.75], x_2 \in [0.05,0.95]\}$. Let the target pollination distribution be

$$\rho_\Omega(\boldsymbol{x}) = 6\cdot\mathbb{1}_{\Gamma_1}(\boldsymbol{x}) + 12\cdot\mathbb{1}_{\Gamma_2}(\boldsymbol{x}) \tag{75}$$

which is shown in the top left of Fig. 4. The other simulation parameters are $\boldsymbol{X}_0 = (0.4,0.2), T = 240, k_f = 0.2, D = 0.0005$, $\gamma_d = 0.25$, $v_1^{\min} = v_2^{\min} = -0.01$, $v_1^{\max} = v_2^{\max} = 0.01$, and $\Delta t = 0.5$.

We note that our choice of $\Delta t = 0.5$ is based on empirical tests of a range of Δt values, each of which satisfies the Courant–Friedrichs–Levy condition needed to solve the advection operator in the macroscopic PDE model. We found that the numerical solution of the macroscopic model does not change significantly for $\Delta t \in (0, 1.5]$. This is because, as shown in Fig. 3, the robots' optimized velocity components $v_1(t), v_2(t)$ and pollination rates $k_1(t), k_2(t)$ do not display sharp variations over any time period of 1.5 units, which means that the typical

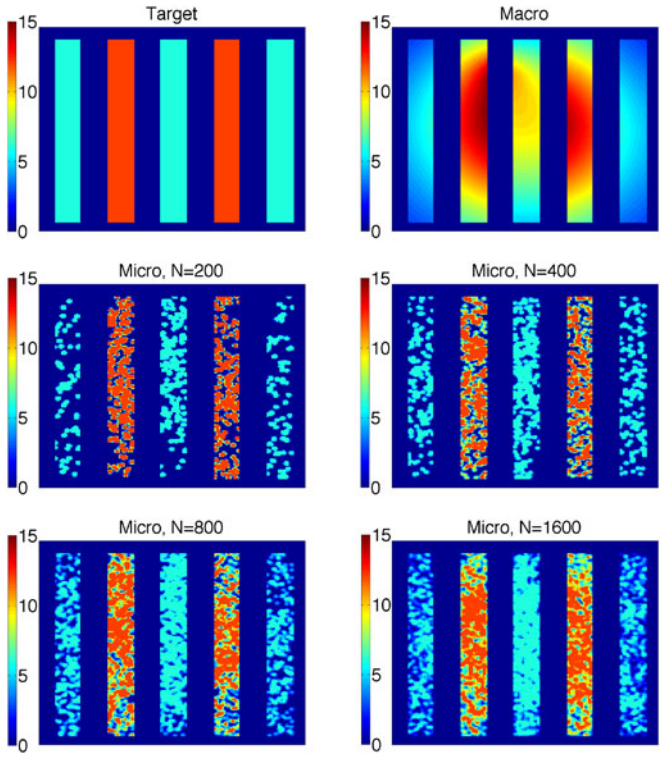

Fig. 4. *Top left*: Target pollination distribution $\rho_\Omega(\boldsymbol{x})$. *Top right*: Expected pollination distribution $\rho_3(\boldsymbol{x}, T)$ from the macroscopic model. *From middle left to bottom right*: Actual pollination distribution $\rho_3^\delta(\boldsymbol{x}, T)$ from the microscopic model with $\delta = 0.015$ and $N = 200$, 400, 800, and 1600 robots. The field is $[0, 1]^2$.

TABLE I
MEAN γ, REL, AND EFFICIENCY FOR EACH VALUE OF N

N	Mean γ	Mean REL	Mean Efficiency
6400	0.1912	0.1968	0.8881
3200	0.2139	0.2636	0.8667
1600	0.2486	0.3601	0.8257
800	0.3065	0.4997	0.7615
400	0.3924	0.7017	0.6643
200	0.5284	0.9845	0.5177

time scales of $v_1(t), v_2(t), k_1(t)$, and $k_2(t)$ are much larger than the time scale resolved with a choice of $\Delta t \in (0, 1.5]$. Furthermore, we note that the choice of Δt has little effect on the error bounds (36) and (37), as explained in Remark VII.2.

2) *Apply the optimal control technique to compute the robot control policies.* Using the parameters above, we run the optimal control technique described in Section VI to compute the robots' velocity $\boldsymbol{v}(t)$ and pollination rates $k_1(t)$ and $k_2(t)$, which are plotted in Fig. 3.

3) *Simulate the microscopic model.* We simulate the microscopic model with the optimized values of $\boldsymbol{v}(t), k_1(t)$, and $k_2(t)$ from Step 2 and the robot sensing radius $\delta = 0.015$. While the design procedure only requires simulations for two distinct values of the swarm size N, here, we simulate the microscopic model for all the values of N shown in Table I. We run 100 simulation trials for each value of N.

4) *Compute the discrepancy γ between the actual and target pollination distributions.* For each simulation of the microscopic model, we compute the resulting actual pollination density field, $\rho_3^\delta(\boldsymbol{x}, T)$, and calculate the discrepancy γ from (70), the relative error REL from (69), and the efficiency from (71). Table I shows the mean γ, REL, and efficiency for each value of N over 100 simulation trials.

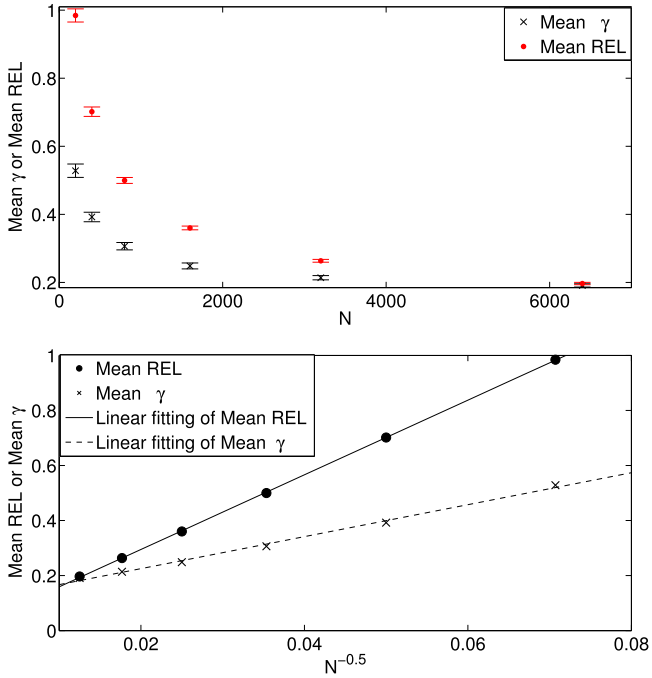

Fig. 5. *Top figure*: Swarm size N versus mean REL and mean γ, both averaged over 100 simulations of the microscopic model for each value of N. The corresponding standard deviations are shown as error bars. *Bottom figure*: $1/\sqrt{N}$ versus mean REL and mean γ. The solid and dashed lines are the linear fittings of mean REL and mean γ, respectively.

Note that as the swarm size N increases, the mean values of γ and REL decrease. This is due to the convergence of the actual pollination density $\rho_3^\delta(\boldsymbol{x}, T)$ to the expected pollination density $\rho_3(\boldsymbol{x}, T)$ with increasing N. We illustrate this convergence in Fig. 4, which plots $\rho_3^\delta(\boldsymbol{x}, T)$ resulting from several values of N (one simulation trial per N) alongside $\rho_3(\boldsymbol{x}, T)$ and the target distribution $\rho_\Omega(\boldsymbol{x})$. To obtain $\rho_3(\boldsymbol{x}, T)$, we numerically solved the macroscopic model over the domain $\bar{\Omega} = [-1, 2]^2$ with $h = 0.006$. The intrinsic discrepancy for this scenario was computed to be $\gamma_\Omega = 0.1413$.

5) *Estimate the required N such that the discrepancy γ is less than γ_d.* From Corollary VII.8, we have that

$$\gamma \leq c_1' + c_2' \frac{\ln N}{\sqrt{N}} \tag{76}$$

where c_1' is the error determined by Δt and δ, and c_2' is a coefficient that depends on δ. Since

$$\ln N \ll N$$

when N is sufficiently large, we conjecture that

$$\gamma = c_1 + c_2 \frac{1}{\sqrt{N}}. \tag{77}$$

In the bottom subfigure of Fig. 5, the linear fitting of mean γ against $1/\sqrt{N}$ verifies (77). This figure also shows that there is a linear relationship between the mean value of REL and $1/\sqrt{N}$.

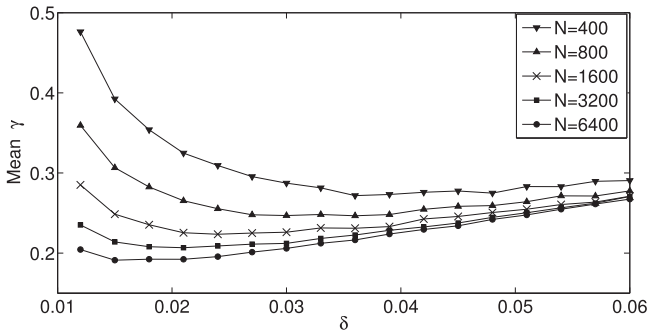

Fig. 6. Relationship among δ, N, and γ. Each data point is averaged over 100 simulations of the microscopic model with the corresponding values of N and δ.

Now, for $\gamma_d = 0.25$, we show how to select the number of robots that are needed to achieve the specification (73). We solve for c_1 and c_2 in (77) using the mean γ for $N_1 = 200$ and $N_2 = 400$ from Table I. The resulting two equations

$$0.5284 = c_1 + c_2 \frac{1}{\sqrt{N_1}}, \quad 0.3924 = c_1 + c_2 \frac{1}{\sqrt{N_2}} \tag{78}$$

yield $c_1 = 0.06407$ and $c_2 = 6.567$. We plug these coefficients into (77) and choose the smallest N such that

$$\gamma \leq \gamma_d = 0.25.$$

This yields $N \approx 1249$.

Remark VIII.1: The robots in this scenario act independently of one another, since there are no interactions such as communication. Hence, a swarm with a large population N will achieve the same distribution of pollination over one deployment as a swarm with a smaller population of αN, $\alpha \in (0, 1)$, over α^{-1} deployments. This deployment strategy can be used when the required value of N for some γ_d exceeds the number of available robots.

6) *Select the value of δ that yields the minimum γ for the required N.* For the selected value of N, there exists an optimal value of δ that yields a minimum value of the discrepancy γ for that N. We illustrate this in Fig. 6, which plots the mean value of γ over 100 simulation trials with respect to different pairs of δ and N. We note that the range of δ in our study and the choice of $\Delta t = 0.5$ yield a very small error (< 0.01) in the operating splitting method (29).

Fig. 6 reflects a tradeoff in choosing δ that is predicted by our error analysis: for a given swarm size N, small δ yield a low coverage outflow near the crop boundary but a high coverage insufficiency, whereas large δ yield a high coverage outflow and a low coverage insufficiency. As the plot shows, the optimal δ becomes smaller as the swarm size N increases. From Step 5, we find that $N \approx 1249$ is the smallest N for which the discrepancy does not exceed γ_d. Thus, we can choose any $N > 1249$, such as $N = 1600$. Then, from Fig. 6, we can pick the optimal δ for $N = 1600$ to further decrease the discrepancy, which gives us $\delta \approx 0.024$ and $\gamma \approx 0.23$. In practice, the sensor limitations will impose an upper bound on δ that may be lower than the optimal value. For example, if we choose $N = 1600$ and the possible range of δ for the sensor is $[0, 0.020]$, then according to Fig. 6, we should choose δ to be 0.020 instead of 0.024.

We further illustrate the effect of δ with the results in Fig. 7, which plots $\rho_3^\delta(\boldsymbol{x}, T)$ resulting from a relatively small robot

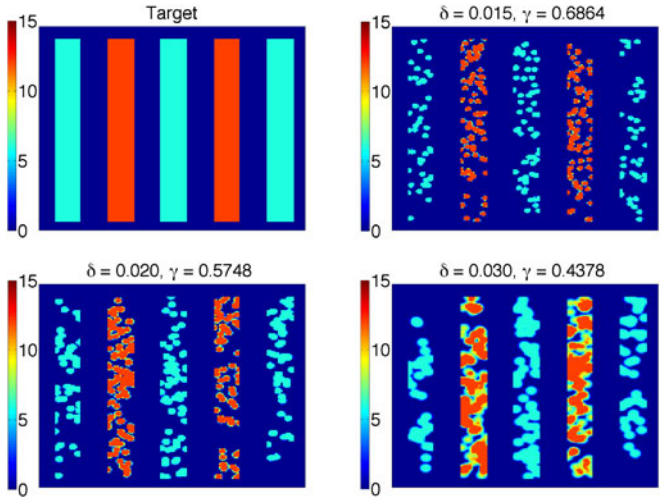

Fig. 7. *Top left*: Target pollination distribution $\rho_\Omega(\boldsymbol{x})$. *From top right to bottom right*: Actual pollination distribution $\rho_3^\delta(\boldsymbol{x}, T)$ from the microscopic model with $N = 100$ robots and $\delta = 0.015$, 0.020, and 0.030. The discrepancy γ is shown for each value of δ. The field is $[0, 1]^2$.

population $N = 100$ and several values of δ (one simulation trial per δ) alongside the target distribution $\rho_\Omega(\boldsymbol{x})$. The figure shows that when N is fixed at 100, the discrepancy γ is very large and coverage is fairly sparse when $\delta = 0.015$, and increasing δ to 0.030 yields a lower discrepancy and improved coverage.

IX. Conclusion

In this work, we derived analytical bounds on the error between a target spatial distribution of coverage activity and the actual coverage distribution that is achieved by a swarm of N robots whose population dynamics can be described by an ADR PDE. We consider scenarios in which the environment is known and the robots' capabilities are highly constrained, in that they have no interrobot communication or global position information. The analytical bound revealed an almost linear relationship between the coverage error and $N^{-\frac{1}{2}}$, thus providing a convenient way to choose a swarm size that produces a coverage distribution within a maximum allowable error. Our analysis also indicated the existence of an optimal robot sensing radius that minimizes the discrepancy between the actual and target coverage distributions for each swarm size, which provides a theoretical basis for selecting a particular sensing range. We verified our analytical results through simulations of a crop pollination scenario. We hope that the detailed analysis presented here will inspire the analysis and design of other distributed systems with a significant stochastic component.

In future work, we are interested in extending our error analysis to models of robotic swarms with pairwise interaction rules between robots, such as collision avoidance maneuvers. This extension will require additional interaction terms in the macroscopic PDE model of the swarm dynamics.

Appendix A

We consider a reduced objective functional $\hat{J}$ corresponding to J in the optimal control problem (34). We define the following

reduced problem:

$$\Xi : U_{ad} \to Y, \quad \min_{\boldsymbol{u}\in U_{ad}} \hat{J}(\boldsymbol{u}) := J(\Xi(\boldsymbol{u}), \boldsymbol{u})$$

where Ξ is a control-to-state mapping, which maps a control, $\boldsymbol{u}$, to $\boldsymbol{\rho}$, the corresponding solution of the macroscopic model (20), (21). The directional derivative of $\hat{J}$ is used in a gradient descent method to numerically compute the optimal robot control parameters. The expression for this derivative is given in the following claim, which is proved in [13].

Claim A.1: The reduced objective functional $\hat{J}$ is directionally differentiable along each $\boldsymbol{h} \in L^\infty(0,T)^{n_f+2}$, where $L^\infty(0,T)$ is the space of essentially bounded functions on the interval $(0,T)$. The directional derivative of $\hat{J}$ has the form

$$d\hat{J}(\boldsymbol{u})\boldsymbol{h} = \int_0^T \langle \sum_{i=1}^{n_f+2} h_i B_i \rho, \boldsymbol{y}\rangle_{L^2(\mathbb{R}^2)^3} + \lambda \langle \boldsymbol{u}, \boldsymbol{h}\rangle_{L^2(0,T)^{n_f+2}}$$

where $\boldsymbol{y}$ is the solution of the backward-in-time adjoint equation

$$-\frac{\partial y_1}{\partial t} = \boldsymbol{v}\cdot\nabla y_1 + D\Delta y_1 + \sum_{j=1}^{n_f} k_j L_j(-y_1+y_2+y_3)$$
$$-\frac{\partial y_2}{\partial t} = k_f y_1 - k_f y_2$$
$$-\frac{\partial y_3}{\partial t} = 0$$

with the final time condition

$$y_1(\boldsymbol{x},T) = y_2(\boldsymbol{x},T) = 0,\ y_3(\boldsymbol{x},T) = \rho_3(\boldsymbol{x},T) - \rho_\Omega(\boldsymbol{x})$$

and the input operators $\{B_i\}$ defined as

$$B_1 = \begin{bmatrix} -\frac{\partial}{\partial x_1} & 0 & 0 \\ 0 & 0 & 0 \\ 0 & 0 & 0 \end{bmatrix}, B_2 = \begin{bmatrix} -\frac{\partial}{\partial x_2} & 0 & 0 \\ 0 & 0 & 0 \\ 0 & 0 & 0 \end{bmatrix}$$
$$B_i = \begin{bmatrix} -L_{i-2} & 0 & 0 \\ L_{i-2} & 0 & 0 \\ L_{i-2} & 0 & 0 \end{bmatrix}, 3 \le i \le n_f+2.$$

The solution $\boldsymbol{y}$ of the above PDE plays the role of the covector in optimal control theory. However, a straightforward application of the maximum principle for finite-dimensional control systems to infinite-dimensional systems is not possible in general. Although there does exist a more general maximum principle for infinite-dimensional control systems such as those governed by PDEs [14], this result is not applicable to our system due to the unboundedness of the control operators B_1 and B_2. An alternative approach to derive necessary conditions based on the first-order derivative of the control-to-state map is to use the Lagrange multiplier technique to formally derive the optimality conditions and then rigorously prove the necessity of these conditions and the differentiability of the control-to-state map. This approach is outlined in [30] and was applied in our prior work [13].

APPENDIX B

Claim B.1: Let $Y_i(\boldsymbol{x})$ be defined as in (48). Then, for each $i = 1, ..., N$ and each $\boldsymbol{x}$,

$$E(Y_i(\boldsymbol{x})) = 0.$$

Proof: Note that if $i \in F_{m+1}$,

$$\begin{aligned} &E\left(G_\delta(\boldsymbol{x} - \boldsymbol{X}_{m+1}^i)\right) \\ &= E\left\{E\left[G_\delta\left(\boldsymbol{x} - \boldsymbol{X}_m^i - \boldsymbol{v}(t_m)\Delta t - \sqrt{2D\Delta t}\Delta \boldsymbol{Z}_m\right)\Big| \boldsymbol{X}_m^i\right]\right\} \\ &= E\left[\int_{\mathbb{R}^2} G_\delta\left(\boldsymbol{x} - \boldsymbol{X}_m^i - \boldsymbol{v}(t_m)\Delta t - \boldsymbol{y}\right)\frac{1}{4\pi D\Delta t} e^{-\frac{|\boldsymbol{y}|^2}{4D\Delta t}} d\boldsymbol{y}\right] \\ &= E\left[\int_{\mathbb{R}^2} G_\delta(\boldsymbol{y}' - \boldsymbol{X}_m^i)\frac{1}{4\pi D\Delta t} e^{-\frac{|\boldsymbol{x} - \boldsymbol{v}(t_m)\Delta t - \boldsymbol{y}'|^2}{4D\Delta t}} d\boldsymbol{y}'\right] \\ &= E\left[\int_{\mathbb{R}^2} G_\delta(\boldsymbol{y} - \boldsymbol{X}_m^i) p(\boldsymbol{x}, t_{m+1}|\boldsymbol{y}, t_m) d\boldsymbol{y}\right] \end{aligned}$$

where we applied the change of variable $\boldsymbol{y}' = \boldsymbol{x} - \boldsymbol{v}(t_m) - \boldsymbol{y}$. This proves our statement for $i \in F_{m+1}$. In addition, $Y_i(\boldsymbol{x}) = 0$ for each $i \notin F_{m+1}$. ■

Claim B.2: For each $i = 1, ..., N$,

$$\|\nabla Y_i(\cdot)\|_\infty \le \frac{C}{N}\sqrt{D}\Delta t \delta^{-4} \ln N$$

with probability greater than $1 - \exp\left[-\frac{1}{2}\Delta t(\ln N)^2\right]$, where C is an independent constant.

Proof: It is straightforward to see that for each $i \in \cup_j H_{j,m+1}$, $\nabla Y_i(\boldsymbol{x}) = 0$. For each $i \in F_{m+1}$,

$$\begin{aligned} \nabla Y_i(\boldsymbol{x}) = &\frac{1}{N}\int_{\mathbb{R}^2} \nabla G_\delta(\boldsymbol{x}' - \boldsymbol{y}) p(\boldsymbol{y}; \Delta t) d\boldsymbol{y} \\ &- \frac{1}{N}\nabla G_\delta(\boldsymbol{x}' - \sqrt{2D\Delta t}\Delta \boldsymbol{Z}_m) \end{aligned}$$

where

$$\boldsymbol{x}' = \boldsymbol{x} - \boldsymbol{v}(t_m)\Delta t - \boldsymbol{X}_m^i$$
$$p(\boldsymbol{y}; \Delta t) = \frac{1}{4\pi D\Delta t}\exp\left(-\frac{|\boldsymbol{y}|^2}{4D\Delta t}\right).$$

Note that

$$|\nabla Y_i(\boldsymbol{x})| \le W_1 + W_2$$

with

$$\begin{aligned} W_1 = &\frac{1}{N}\int_{\mathbb{R}^2} |\nabla G_\delta(\boldsymbol{x}' - \boldsymbol{y}) \\ &- \nabla G_\delta(\boldsymbol{x}' - \sqrt{2D\Delta t}\Delta \boldsymbol{Z}_m - \boldsymbol{y})| \cdot p(\boldsymbol{y}; \Delta t) d\boldsymbol{y} \\ W_2 = &\frac{1}{N}\Big| \int_{\mathbb{R}^2} \nabla G_\delta(\boldsymbol{x}' - \sqrt{2D\Delta t}\Delta \boldsymbol{Z}_m - \boldsymbol{y}) p(\boldsymbol{y}; \Delta t) d\boldsymbol{y} \\ &- \nabla G_\delta(\boldsymbol{x}' - \sqrt{2D\Delta t}\Delta \boldsymbol{Z}_m)\Big| \end{aligned}$$

Since $\Delta \boldsymbol{Z}_m = (\Delta Z_m^1, \Delta Z_m^2) \sim \boldsymbol{W}(0,1)$,

$$P\left(\max_{i=1,2} |\Delta Z_m^i| \le \sqrt{\Delta t \ln N}\right) \ \ge \ 1 - \exp\left[-\frac{1}{2}\Delta t (\ln N)^2\right].$$

By the mean value theorem

$$\begin{aligned} W_1 &= \frac{1}{N}\int_{\mathbb{R}^2} \left|\partial^2 G_\delta(\xi_1(\boldsymbol{x},\boldsymbol{y}))\sqrt{2D\Delta t}\Delta \boldsymbol{Z}_m p(\boldsymbol{y};\Delta t)\right| \boldsymbol{dy} \\ &\le \ \frac{2\sqrt{2D\Delta t}}{N} \max_{i,j=1,2} |\partial_{x_i x_j} G_\delta| \max_{i=1,2} |\Delta Z_m^i| \qquad (79) \\ &\le \ \frac{C'}{N}\sqrt{D}\Delta t \delta^{-4} \ln N \end{aligned}$$

with probability greater than $1 - \exp\left[-\frac{1}{2}\Delta t(\ln N)^2\right]$. Here, C' is an independent constant.

Now, we estimate W_2. It is straightforward to see that

$$W_2 \ \le \ \|\nabla G_\delta * p - \nabla G_\delta\|_\infty.$$

By using a change of variable $\boldsymbol{y} = \sqrt{\Delta t}\boldsymbol{y}'$, we obtain

$$\begin{aligned} G_\delta * p(\boldsymbol{x};\Delta t) - G_\delta(\boldsymbol{x}) = \int_{\mathbb{R}^2} \Big[&-\partial^2 G_\delta(\boldsymbol{x})\sqrt{\Delta t}\boldsymbol{y}' \\ &+ \frac{1}{2}\Delta t \partial^3 G_\delta(\xi_2(\boldsymbol{x},\boldsymbol{y}'))|\boldsymbol{y}'|^2\Big] \cdot p(\boldsymbol{y}';1)\boldsymbol{dy}'. \end{aligned}$$

Applying the facts that

$$\int_{\mathbb{R}^2} \boldsymbol{y}' p(\boldsymbol{y}';1)\boldsymbol{dy}' = 0, \quad \max_{i,j,z=1,2} |\partial_{x_i x_j x_z} G_\delta| \ \le \ C\delta^{-5}$$

we have that

$$W_2 \ \le \ \|\nabla G_\delta * p - \nabla G_\delta\|_\infty \ \le \ C''\Delta t \delta^{-5} \qquad (80)$$

where C'' is an independent constant. Combining (79) and (80), and noting that $N \gg \delta^{-1}$, we arrive at

$$\|\nabla Y_i(\cdot)\|_\infty \ \le \ \frac{C}{N}\sqrt{D}\Delta t \delta^{-4} \ln N$$

with probability greater than $1 - \exp\left[-\frac{1}{2}\Delta t(\ln N)^2\right]$. ■

Claim B.3: The following inequality holds:

$$\|EM(\cdot)\|_{1,\bar{\Omega}^c} \ \le \ \Delta t^2.$$

Proof: By our assumptions in Theorem VII.1, $\exists \zeta > 0$ such that $\boldsymbol{X}_m^i \in \bar{\Omega}_{\text{in}}^{2\zeta}$ and $\delta < \zeta$. Since $G_\delta(\boldsymbol{x})$ is supported in B_δ,

$$G_\delta(\boldsymbol{x} - \boldsymbol{X}_m^i) = 0 \quad \forall \boldsymbol{x} \notin \bar{\Omega}_{\text{in}}^{\zeta}, \ \forall m = 1,...,M, \ i = 1,...,N.$$

Therefore, we have

$$\begin{aligned} \|Y_i(\cdot)\|_{1,\bar{\Omega}^c} = \frac{1}{N}\int_{\bar{\Omega}^c}\int_{\bar{\Omega}_{\text{in}}^{\zeta}} &G_\delta(\boldsymbol{y} - \boldsymbol{X}_m^i) p(\boldsymbol{x}, t_{m+1}|\boldsymbol{y}, t_m) \\ &\cdot \boldsymbol{dy}\boldsymbol{dx}. \end{aligned}$$

By definition, $\forall \boldsymbol{x} \in \bar{\Omega}^c, \boldsymbol{y} \in \bar{\Omega}_{\text{in}}^{\zeta}$, $|\boldsymbol{x} - \boldsymbol{y}| \ge \zeta$. Thus, we can choose Δt small enough so that $|\boldsymbol{x} - \boldsymbol{y} - v(t_m)\Delta t| \ge \frac{\zeta}{2}$. Defining $B_\zeta = \{\boldsymbol{x} : |\boldsymbol{x}| \le \zeta\}$, we have

$$\begin{aligned} &\|Y_i(\cdot)\|_{1,\bar{\Omega}^c} \\ &\le \ \frac{1}{N}\int_{\bar{\Omega}_{\text{in}}^{\zeta}} G_\delta(\boldsymbol{y} - \boldsymbol{X}_m^i)\boldsymbol{dy} \int_{(B_{\zeta/2})^c} \frac{1}{4\pi D\Delta t} e^{-\frac{|\boldsymbol{x}|^2}{4D\Delta t}} \boldsymbol{dx} \\ &\le \ \frac{1}{N}\int_{\zeta/2}^{\infty} \frac{r}{2D\Delta t} e^{-\frac{r^2}{4D\Delta t}} \boldsymbol{dr} = \frac{1}{N} e^{-\frac{\zeta^2}{16D\Delta t}} \ \le \ \frac{\Delta t^2}{N} \end{aligned}$$

since $\Delta t \ll \zeta$. Hence

$$\|\text{EM}(\cdot)\|_{1,\bar{\Omega}^c} \ \le \ \sum_{i=1}^{N} \|Y_i(\cdot)\|_{1,\bar{\Omega}^c} \ \le \ \Delta t^2.$$

■

Claim B.4: The inequality

$$\sum_{i=1}^{N} |\varphi_i| \ \le \ 2\Delta t K$$

is true with probability greater than $1 - 2\exp[-C\Delta t K N/2]$, where C is an independent constant.

Proof: We define

$$\varphi_i' = |\varphi_i| - E(|\varphi_i|).$$

Then, $E(\varphi_i') = 0$ and $E(|\varphi_i|) \le \Delta t K N^{-1}$. Applying Bennett's inequality (50) with $\eta = \Delta t K$, $M_0 = N^{-1}$, and $V = \Delta t K N^{-1}$, we obtain

$$P\left(\left|\sum_{i=1}^{N} \varphi_i'\right| \ge \Delta t K\right) \ \le \ 2\exp\left[-B(1)\Delta t K N/2\right].$$

Hence

$$\sum_{i=1}^{N} |\varphi_i| \ \le \ \left|\sum_{i=1}^{N} \varphi_i'\right| + \sum_{i=1}^{N} E(|\varphi_i|) \ \le \ 2\Delta t K$$

with probability greater than $1 - 2\exp[-B(1)\Delta t K N/2]$. ■

REFERENCES

[1] A Roadmap for U.S. Robotics: From Internet to Robotics, 2013. [Online]. Available: http://robotics-vo.us/sites/default/files/2013%20Robotics%20Roadmap-rs.pdf

[2] M. Annunziato and A. Borzì, "A Fokker–Planck control framework for multidimensional stochastic processes," *J. Comput. Appl. Math.*, vol. 237, no. 1, pp. 487–507, 2013.

[3] J. Beal and M. Viroli, "Space–time programming," *Philosoph. Trans. Roy. Soc. London A, Math., Phys. Eng. Sci.*, vol. 373, 2015, Art. no. 2046.

[4] G. Bennett, "Probability inequalities for the sum of independent random variables," *J. Amer. Statist. Assoc.*, vol. 57, no. 297, pp. 33–45, 1962.

[5] A. Bensoussan, J. Frehse, and P. Yam, *Mean Field Games and Mean Field Type Control Theory*, vol. 101. New York, NY, USA: Springer-Verlag, 2013.

[6] E. Bonabeau, M. Dorigo, and G. Theraulaz, *Swarm Intelligence: From Natural to Artificial Systems* (ser. SFI Studies in the Science of Complexity). New York, NY, USA: Oxford Univ. Press, 1999.

[7] M. Brambilla, E. Ferrante, M. Birattari, and M. Dorigo, "Swarm robotics: A review from the swarm engineering perspective," *Swarm Intell.*, vol. 7, pp. 1–41, 2013.

[8] C. Canuto, F. Fagnani, and P. Tilli, "A Eulerian approach to the analysis of Rendez-Vous algorithms," in *Proc. 17th IFAC World Congr.*, 2008, pp. 9039–9044.

[9] T. H. Chung, M. R. Clement, M. A. Day, K. D. Jones, D. Davis, and M. Jones, "Live-fly, large-scale field experimentation for large numbers of fixed-wing UAVs," in *Proc. IEEE Int. Conf. Robot. Autom.*, May 2016, pp. 1255–1262.

[10] R. M. Colombo and N. Pogodaev, "Confinement strategies in a model for the interaction between individuals and a continuum," *SIAM J. Appl. Dyn. Syst.*, vol. 11, no. 2, pp. 741–770, 2012.
[11] K. Craig and A. L. Bertozzi, "A blob method for the aggregation equation," *Math. Comput.*, vol. 85, no. 300, pp. 1681–1717, 2016.
[12] K. Elamvazhuthi, C. Adams, and S. Berman, "Coverage and field estimation on bounded domains by diffusive swarms," in *Proc. IEEE Conf. Decision Control*, 2016, pp. 2867–2874.
[13] K. Elamvazhuthi and S. Berman, "Optimal control of stochastic coverage strategies for robotic swarms," in *Proc. IEEE Int. Conf. Robot. Autom.*, 2015, pp. 1822–1829.
[14] H. O. Fattorini, *Infinite Dimensional Optimization and Control Theory*, vol. 54. Cambridge, U.K.: Cambridge Univ. Press, 1999.
[15] M. Fornasier and F. Solombrino, "Mean-field optimal control," *ESAIM: Control, Optim. Calculus Variations*, vol. 20, no. 4, pp. 1123–1152, 2014.
[16] A. Griffiths, A. Dikarev, P. R. Green, B. Lennox, X. Poteau, and S. Watson, "AVEXIS—Aqua vehicle explorer for in-situ sensing," *IEEE Robot. Autom. Lett.*, vol. 1, no. 1, pp. 282–287, Jan. 2016.
[17] H. Hamann and H. Wörn, "A framework of space–time continuous models for algorithm design in swarm robotics," *Swarm Intell.*, vol. 2, nos. 2–4, pp. 209–239, 2008.
[18] W. Hoeffding, "Probability inequalities for sums of bounded random variables," *J. Amer. Statist. Assoc.*, vol. 58, no. 301, pp. 13–30, 1963.
[19] J.-M. Lasry and P.-L. Lions, "Mean field games," *Jpn. J. Math.*, vol. 2, no. 1, pp. 229–260, 2007.
[20] K. Y. Ma, P. Chirarattananon, S. B. Fuller, and R. J. Wood, "Controlled flight of a biologically inspired, insect-scale robot," *Science*, vol. 340, no. 6132, pp. 603–607, 2013.
[21] A. J. Majda and A. L. Bertozzi, *Vorticity and Incompressible Flow*, vol. 27. Cambridge, U.K.: Cambridge Univ. Press, 2002.
[22] A. R. Mesquita and J. P. Hespanha, "Jump control of probability densities with applications to autonomous vehicle motion," *IEEE Trans. Automat. Control*, vol. 57, no. 10, pp. 2588–2598, Oct. 2012.
[23] D. Milutinovic and P. Lima, "Modeling and optimal centralized control of a large-size robotic population," *IEEE Trans. Robot.*, vol. 22, no. 6, pp. 1280–1285, Dec. 2006.
[24] A. Okubo and S. A. Levin, *Diffusion and Ecological Problems: Modern Perspectives*, vol. 14. New York, NY, USA: Springer, 2013.
[25] G. A. Pavliotis, *Stochastic Processes and Applications* (ser. Texts in Applied Mathematics), vol. 60. New York, NY, USA: Springer-Verlag, 2014.
[26] B. Piccoli, F. Rossi, and E. Trélat, "Control to flocking of the kinetic Cucker–Smale model," *SIAM J. Math. Anal.*, vol. 47, no. 6, pp. 4685–4719, 2015.
[27] A. Prorok, N. Correll, and A. Martinoli, "Multi-level spatial modeling for stochastic distributed robotic systems," *Int. J. Robot. Res.*, vol. 30, no. 5, pp. 574–589, 2011.
[28] C. Robin and S. Lacroix, "Multi-robot target detection and tracking: Taxonomy and survey," *Auton. Robots*, vol. 40, pp. 729–760, 2016.
[29] S. Tong, E. J. Fine, Y. Lin, T. J. Cradick, and G. Bao, "Nanomedicine: Tiny particles and machines give huge gains," *Ann. Biomed. Eng.*, vol. 42, no. 2, pp. 243–259, 2014.
[30] F. Tröltzsch, *Optimal Control of Partial Differential Equations: Theory, Methods and Applications* (ser. Graduate Studies in Mathematics), vol. 112. Providence, RI, USA: Amer. Math. Soc., 2010.

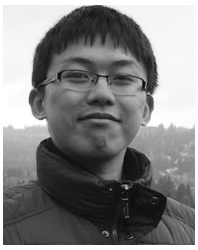

Fangbo Zhang received the B.S. degree in mathematics from Shanghai Jiao Tong University, Shanghai, China, in 2013. He is currently working toward the Ph.D. degree in mathematics with the University of California, Los Angeles (UCLA), Los Angeles, CA, USA.

Since 2013, he has been a Research and Teaching Assistant with the Department of Mathematics, UCLA. His current research interests include analysis of swarm models, machine learning, and partial differential equations.

Andrea L. Bertozzi received the B.A., M.A., and Ph.D. degrees in mathematics from Princeton University, Princeton, NJ, USA, in 1987, 1988, and 1991, respectively.

She was on the faculty of the University of Chicago, Chicago, IL, USA, from 1991 to 1995 and Duke University, Durham, NC, USA, from 1995 to 2004. During 1995–1996, she was the Maria Goeppert-Mayer Distinguished Scholar with Argonne National Laboratory. Since 2003, she has been a Professor of mathematics with the University of California, Los Angeles, where he currently serves as the Director of Applied Mathematics. In 2012, she was appointed the Betsy Wood Knapp Chair for Innovation and Creativity. Her research interests include machine learning, image processing, cooperative control of robotic vehicles, and swarming.

Dr. Bertozzi is a Fellow of the Society for Industrial and Applied Mathematics, the American Mathematical Society, and the American Physical Society. Her past honors include a Sloan Foundation Research Fellowship, the Presidential Career Award for Scientists and Engineers, and the SIAM Kovalevsky Prize in 2009.

Karthik Elamvazhuthi received the B.Tech. degree in mechatronics engineering from Manipal Institute of Technology, Manipal, India, in 2011, and the M.S. degree in mechanical engineering in 2014 from Arizona State University, Tempe, AZ, USA, where he is currently working toward the Ph.D. degree in mechanical engineering.

His current research interests include modeling and control of robotic swarms using methods from partial differential equations and stochastic processes.

Spring Berman (M'07) received the B.S.E. degree in mechanical and aerospace engineering from Princeton University, Princeton, NJ, USA, in 2005, and the M.S.E. and Ph.D. degrees in mechanical engineering and applied mechanics from the University of Pennsylvania, Philadelphia, PA, USA, in 2008 and 2010, respectively.

From 2010 to 2012, she was a Postdoctoral Researcher in computer science with Harvard University, Cambridge, MA, USA. Since 2012, she has been an Assistant Professor of mechanical and aerospace engineering with the School for Engineering of Matter, Transport and Energy, Arizona State University, Tempe, AZ, USA. Her research focuses on the modeling and analysis of behaviors in biological and engineered collectives and the synthesis of control strategies for robotic swarms.

Prof. Berman received the 2014 Defense Advanced Research Projects Agency Young Faculty Award and the 2016 Office of Naval Research Young Investigator Award.